8

Westinghouse Imaging Devices

(NASA-CR-130934) A PROGRAM TO IMPROVE THE WX-5419B SEC CAMERA TUBE FOR LONG INTEGRATION SATELLITE APPLICATIONS Final Report (Westinghouse Electric Corp.) ~~64~~ 66 p HC $4.25 CSCL 09A

N73-19434

G3/14 Unclas 65188

PRICES SUBJECT TO CHANGE

ELECTRONIC TUBE DIVISION
ELMIRA, NEW YORK 14902

FINAL REPORT

ON CONTRACT NO. NSR-31-001-127

SUBCONTRACT NO. 1

FEBRUARY 1972

A PROGRAM TO IMPROVE THE WX-5419B SEC CAMERA TUBE FOR LONG INTEGRATION SATELLITE APPLICATIONS

WESTINGHOUSE ELECTRIC CORPORATION
ELECTRONIC TUBE DIVISION
ELMIRA, NEW YORK 14902

TABLE OF CONTENTS

LIST OF TABLES

LIST OF ILLUSTRATIONS

1.0 INTRODUCTION

The objective of the program of work reported here was to develop an SEC TV camera tube with the following special characteristics.

(a) long integration

(b) ruggedized construction for satellite launching

(c) high resolution

(d) UV transmissive input window

Prior to the start of the program of work, experimental tests with the magnetically focused SEC camera tube, type WX-5419B manufactured by Westinghouse had shown that this tube was capable of storing electrical charges in its target for periods of many hours. It had also been experimentally established that the dark current in this tube could be kept sufficiently low to permit integration of weak signals for periods of up to ten hours, and that after such a period of integration, the accumulated charge could be read out in a single sweep of the scanning beam. These features and the high resolution of the tube over the entire scanned area made this tube type potentially suitable for astronomical type applications where long integration times and high storage capacity, together with high sensitivity and resolving power were essential requirements. In order to increase the signal to noise ratio and to reduce band width requirements, operation at slow scanning rates of several seconds per frame was also required.

The WX-5419B type of SEC camera tube thus had the potential for satisfying the tube requirements established at the start of the present program. Some design modifications, however, were required, and three major areas were identified for improvement. These were:

(1) The gun required a light shield in order to avoid the generation of a background current caused by light from the thermionic filaments reaching the photocathode.

(2) Elimination of the suppressor mesh was required since the presence of a suppressor mesh in the standard WX-5419B caused excessive microphonics, target mesh touches, reduced resolution and increased the target shunt capacity and, thus, the noise level of the system. Finally the suppressor mesh effectively increased the amount of beam current required to discharge the target. However, removal of the suppressor mesh required that some means be provided to prevent "crossing over" the target.

(3) Means for reducing the dark current further were also required. These included reduction of high field strength concentrations, polishing and smoothing of metal parts and the use of a bi-alkali photocathode in place of the standard S-20 type of photocathode (this is only permissible for applications in which operation at wave lengths of less than 6,000 angstroms is required).

(4) Since operation at wave lengths ranging from the short ultra-violet (1150 angstroms) to the visible region was specified, the tube also required a suitable UV transmitting input window.

The objective of the program of work was to develop a magnetically focused and deflected SEC camera tube with a ruggedized design which could withstand satellite launching, which incorporated an ultra-violet transmissive window and which had a bi-alkali photocathode. The target area required was 25mm x 25mm. The target was to be a high gain and a high capacity type which would not cross over when facing a field mesh potential of several hundred volts. A dark current as low as possible was required which, in turn, required completely stable and corona free high voltage operation for image section voltages of up to 10,000 volts. Finally, microphonics and target shunt capacity were also required to be as low as possible.

2.0 PROGRAM OF WORK

2.1 General Design and Areas of Special Experimentation

The SEC camera tube to be developed was designated the WX-31718. At the beginning of the program of work it was planned to start with the design of the ruggedized version of the WX-5419B (the WX-31222) and modify the electrodes in order to avoid sharp edges and areas of high field concentration. It was also decided to use an input window made from a single crystal of MgF_2 sealed to the tube by a technique developed for the Uvicon camera tube. It was also decided to conduct shock and sinusoidal vibration tests on samples of the WX-31222 in order to identify potential weak points in its design. The vibration requirements corresponded approximately to those used during the Uvicon tests. One of the WX-31222 tubes was shock tested at 8.5 g's for a duration of 11 milliseconds. The potassium chloride of the target showed a crack together with some loss of KCl. Two other tubes were vibrated up to levels of 10g between 100 and 150 Hz in the direction of the tube's longitudinal axis. The highest g level in the lateral direction was 5 g's at frequencies between 5 and 150 Hz and 350 and 550 Hz. Neither the target substrate nor the electron gun or other parts of the tube were affected by the vibration. However, these tubes contained suppressor meshes, spaced approximately 10 mils from the KCl target, and the target showed large areas of target damage caused by target to suppressor mesh touches. The tube developed during this program of work (WX-31718) did not contain a suppressor mesh and the spacing between the target and the field mesh (the adjacent mesh) was approximately .250 inches.

These preliminary vibration and shock tests showed that the basic design of the ruggedized WX-31222 was sound but that a tube without a suppressor mesh was required.

Following the vibration tests a new tube (WX-31718) was designed and manufactured containing improved accelerator electrodes and a target mesh assembly without a suppressor mesh. The target support consisted of a rastered structure with an elevated 1" x 1" square rim onto which a substrate could be mounted. The field mesh was welded to a correspondingly rastered mesh support. This first tube was manufactured with a glass faceplate with a bi-alkali photocathode.

Two major problem areas were identified at the beginning of the program of work which required resolving before proceeding with the manufacture of further tubes. The first of these problem areas was the sealing of the MgF_2 window to the tube and the second was the processing of a bi-alkali photocathode on a MgF_2 substrate. These principle problem areas will be discussed in the following two paragraphs.

2.2 Faceplate Assembly

Two materials were considered for use as the input window in order to provide transmission at wave-lengths of 1100 angstroms. These were LiF and MgF_2. Some properties of these two materials are listed in Table 1. The major advantages of MgF_2 compared with LiF are its lower solubility in water (approximately 3% of that of LiF) which permits handling in water and indefinite exposure to humid atmosphere and its much greater hardness, which makes MgF_2 less vulnerable to scratches and provides a better polished surface. As can be seen from Table 1, the linear expansion of MgF_2 is lower than that of LiF and is different for two directions, parallel and normal, to the crystal axis. This is an important point. Figure 1 shows elongation versus temperature for the two axes of the MgF_2 crystal. Also shown in Figure 1 for comparison is the elongation of stainless steel number 430.

Table 1

MATERIAL	LITHIUM FLUORIDE	MAGNESIUM FLUORIDE		CALCIUM FLUORIDE	BARIUM FLUORIDE
UV CUTOFF (MICRONS)	.105	.113		.123	.134
IR CUTOFF (MICRONS)	9.0	7.5		12.0	15.0
SOLUBILITY in H_2O (G/100G H_2O)	0.27 at 18° C	0.0076 at 18° C		1.51×10^{-3} at 20° C	0.21 at 25° C
ELASTIC LIMIT BY FLEXURE (DYNE/CM²)	10.9×10^7			3.70×10^8	2.7×10^8
HARDNESS KNOOP SCALE (KG/MM²)	102	415		158	82
LINEAR EXPANSION (10^{-6}/°C)		Par C axis	⊥ C axis		
—100°C	23.7		—	10.4	18.4
0	32.3	(12) 13.1	8.8	18	18.4
100	36.4		9.45	20	
400	49.2		13.4	28	
MELTING POINT (° C)	846	1255		1402	1320

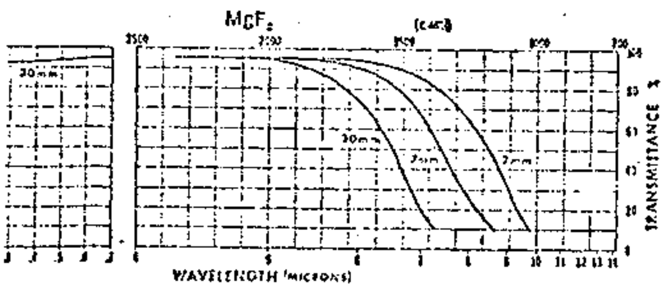

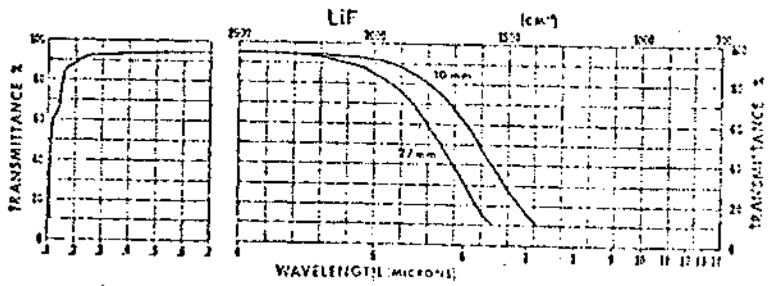

REGULAR QUALITY

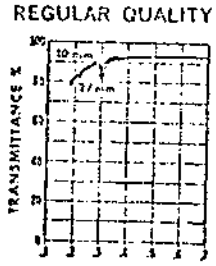

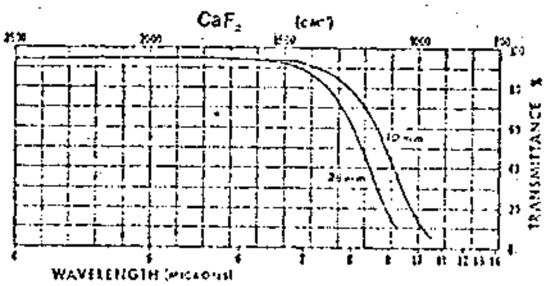

SPECIAL VACUUM U.V. QUALITY

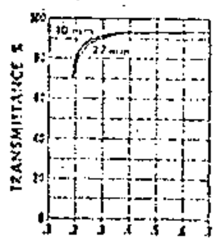

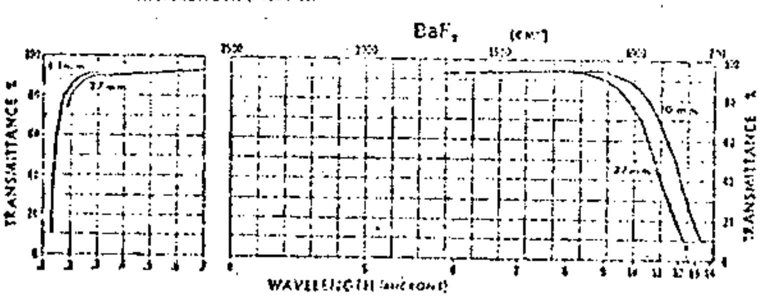

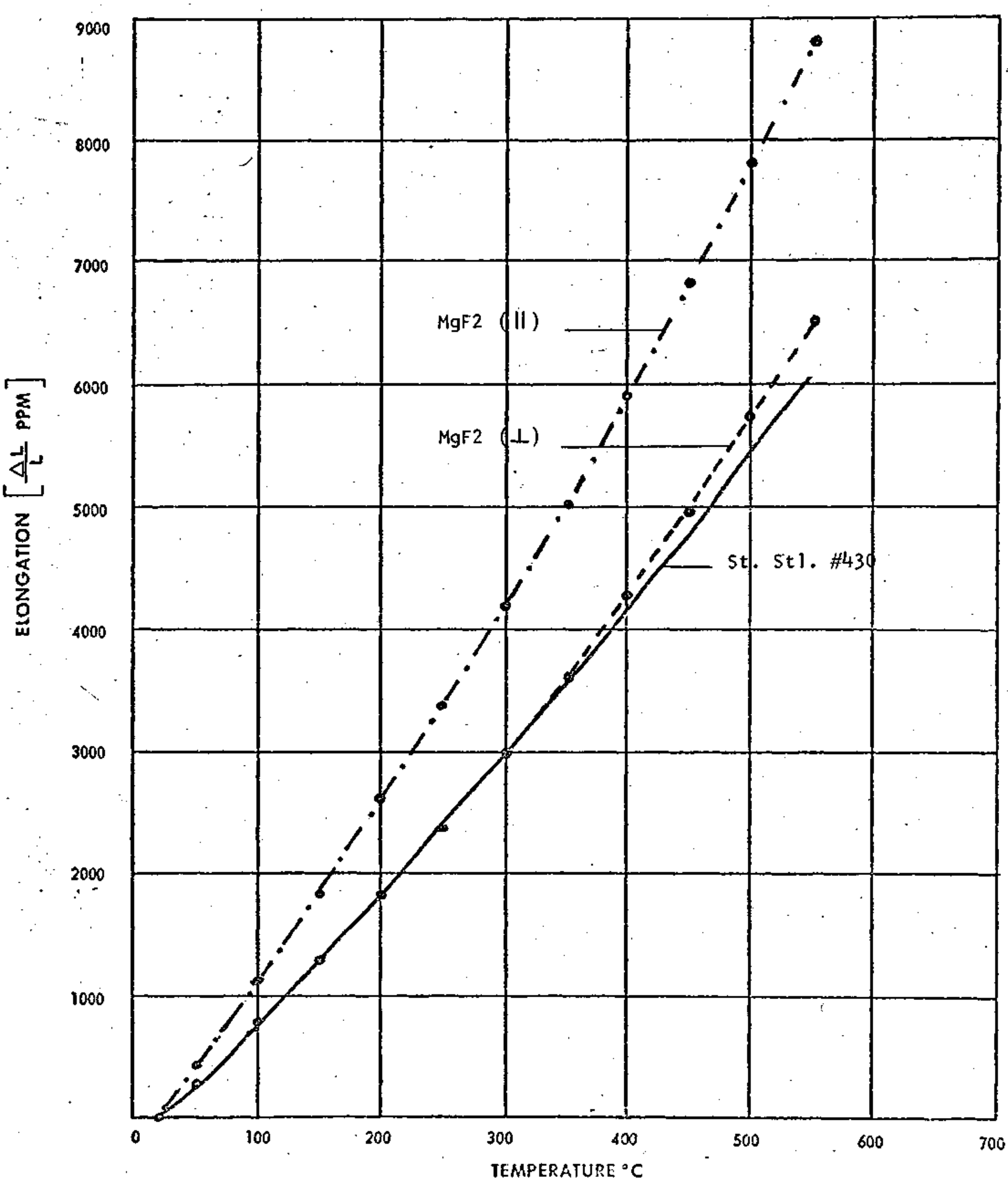
9000
8000
7000
6000
5000
4000
3000
2000
1000
0
100
200
300
400
500
600
700
ELONGATION [ΔL/L PPM]
TEMPERATURE °C
MgF2 (||)
MgF2 (⊥)
St. Stl. #430

Figure 1

During the Uvicon program, Westinghouse had developed a technique for sealing LiF to Kovar flanges. The LiF is not sealed directly onto the Kovar metal but is sealed via a silver sleeve with a feather edged rim. The silver sleeve is braised to the Kovar flange and the crystal is sealed to the silver sleeve by means of silver chloride. See Figure 2. At first, the same procedure was adopted in order to seal the MgF_2 windows to the input sealing flange. Six complete tubes were made using this sealing technique. Each window assembly was leak checked before use on a tube. Three window assemblies had to be re-sealed because of small leaks which developed during the pre-baking process. Pre-baking was a serious cause of leaks. Of the final five tubes, sealed off exhaust, two tubes were leak tight and two further tubes were lost because of small leaks and one other tube was lost by a larger leak in the seal which developed during the exhaust process.

Table 2 lists the expansion co-efficients of several pertinent materials and, as one can see, LiF has a linear expansion which is much closer to silver chloride than to MgF_2. Silver chloride is a malleable material which will accommodate some mis-match in expansion, however, the wetting of the crystal and the adhesion caused some difficulties because silver chloride would not wet the crystal very well and it was necessary to insert between the MgF_2 and the silver chloride a layer of a noble metal such as platinum, gold or silver. Of these, silver proved to be the better material. After evaluation of these initial experiments, the conclusion was arrived at that the technique described was of marginal success and a better method was required.

An inspection of Table 2 and Figure 1 shows that two metals, namely Carpenter 49 and stainless steel number 430 are very close to the expansion of MgF_2, particularly the stainless steel 430. Unfortunately the data pertinent to stainless steel was not discovered until later in the program, and at first,

TABLE II

Material	Exp. Co-Eff. X 10^{+7}	Temperature Range
MgF_2	88	0°C
MgF_2	112	0-400°C
LiF	323	0°C
Silver	200	0-500°C
Silver Chloride	340	20-150°C
Kovar	45	100-400°C
Stainless St. 430	110	0-400°C
Carpenter 49	91.4	0-400°C

some experiments were tried using Carpenter 49 before using stainless steel exclusively. Two techniques were experimented with to seal the MgF_2 crystal to the flange. These were, firstly, a direct seal to the flange using a glass frit as a sealing medium and secondly, a technique which involved the insertion between the crystal and the metal flange of a ductile metal foil, the purpose of which was to prevent the transfer of stress from one material to another. Figure 3 illustrates the principle of this latter technique.

A four to five mil thick gold foil is sealed to a two-step Kovar flange by means of an electron beam welder. The MgF_2 crystal is then soldered using a suitable glass frit onto the gold foil. This work was carried out in cooperation with the Mosaic Division of the Bendix Corporation.

The technique of sealing the MgF_2 crystal directly to the stainless steel flange was successful and two leak-tight assemblies were produced, however, both assemblies cracked during the heli-arc welding of the stainless steel faceplate flange to the Kovar flange of the camera tube image section, and it was decided to continue with the gold foil technique exclusively.

Fifteen window assemblies, in all, were made using the gold foil technique. Of these, eleven were used on complete tubes without any loss caused by leaks in the window seal. One tube was lost by a crack which developed in the glass seal when the tube was inadvertently baked at a temperature of 400°C. The limit for baking is 350°C above which the glass frit separates from the gold foil. The highest baking temperature used on the complete tubes was 325°C, during the application of the glass frit. It was discovered that it was important, to restrict the glass frit to the flat face of the MgF_2 crystal and to keep the glass frit away from the side walls of the crystal. If the glass frit was allowed to encroach on the cylindrical walls of the crystal, the

Featheredge Technique

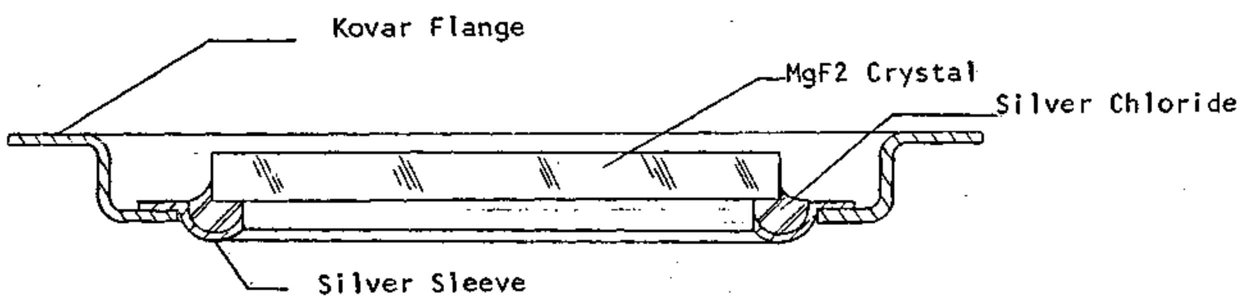

Figure 2

Gold Foil Sealing Technique

Figure 3

larger expansion in this direction caused chipping at the edges of the crystal. It was also discovered that it was important to insure that sufficient space was left between the electron beam welded area and the edge of the crystal to permit expansion of the foil. A too short distance resulted in rupturing of the gold foil. One window assembly was spoiled by cleaning trials in a hydrogen oven. At the termination of the program of work, two spare window assemblies were left. It was concluded that the gold foil technique was a satisfactory procedure for sealing MgF_2 crystals onto Kovar flanges. It is also believed that, with some modification, this technique could be applied to the sealing of other crystals.

2.3 Bi-Alkali Photosurface

One of the most sensitive photosurfaces over a wide spectral range from the far ultraviolet to the near infrared is the S-20 type of photosurface composed of antimony together with the three alkalis: sodium, potassium and cesium. The quantum efficiency of the S-20 photocathode is of the order of 15 to 20 per cent in the wave length range from approximately 4,000 angstroms to the far ultraviolet. The presence of cesium in the image section of the camera tube, however, can cause optical and electron emission under high field strength conditions giving rise to a background current. The principal effect of the cesium, on the photocathode, is to provide photoemission in the red regions of the spectrum and for applications where no red emission is required, the cesium can be emitted. It was, therefore, felt that for the present tube, a bi-alkali photocathode would provide an adequate spectral response, and at the same time, provide a tube with a lower dark current.

A bi-alkali photocathode also has an advantage compared with other photocathodes, such as Cs_2Te and Cs which may be used in the ultra-violet region of the spectrum, of providing better resolution. The explanation for this is as follows: A photon with an energy of less than twice the band gap of Cs_2Te incident upon a Cs_2Te photocathode will give rise to emitted photoelectrons with relatively large emission energies. These large emission energies increase chromatic aberration and cause a reduction in resolution. As the energy of the incident photon increases, the threshold for pair production is reached and a single incident photon can cause the emission of two photoelectrons having low emission energies thus permitting an increase in resolution. The same process is true for the bi-alkali photocathode, however, in this case, because of the bi-alkali photocathode's smaller band gap, the threshold for pair production lies further towards the long wave length region of the spectrum. Thus, the energy of emitted electrons whose emission is caused by photons with energies of less than twice the band gap, is correspondingly less, leading to less chromatic aberration and better resolution.

Because there was no previous experience with the development of bi-alkali photo-surfaces on magnesium fluoride substrates, the first tube was made with a bi-alkali photocathode deposited upon a plain glass substrate in order to establish a photocathode sensitivity reference level. The first tube had a bi-alkali photocathode with a response to white light of 49 μA/l. The following five tubes with MgF_2 faceplates and silver chloride seals measured 30, 26, 33, 10 and 20 μA/l, respectively, giving an average value of 24 μA/l. Unfortunately, at that time, the spectral response or quantum efficiency measurements could not be made in the ultraviolet region of the spectru, thus a possible correlation between quantum efficiency in the ultraviolet region and response of the photocathode to white light could not be determined. A second tube built with a glass faceplate had a response to white light of 63 μA/l. The following three tubes, each of which was manufactured using the gold foil technique, had white light responses of 22, 14 and 8 μA/l respectively, considerably below the values obtained for photocathodes deposited on glass faceplates. It was decided at this point to continue photocathode experimentation in a simpler, reusable vacuum vessel. Using this bottle, 19 photocathode experiments were made, the results of which are shown in Table 3. Very little trend was observed during these experiments. The magnesium fluoride faceplate assemblies were cleaned by a variety of methods involving acids, water, detergents, and alcohol, with no preferred method being discovered.

It did appear, however, that a light glow discharge in a slight oxygen atmosphere improved the white light response of the bi-alkali photocathodes. A thin sub-layer of chromium was used in some photocathodes to decrease the lateral resistivity of the photocathode, although the presence of the chromium did not appear to significantly affect the response, the use of the sub-layer was discontinued. Finally, eight tubes were made. One tube went to air during tip-off. The other seven tubes had white light responses of 9.8, 25, 24, 12, 18, 14 and 10.5 μA/l, respectively, thus providing an average response of 16 μA/l. The photocathode experiments are summarized in Tables 3 and 4.

TABLE III

PHOTO EXPERIMENTS

No.	Date	Faceplate	Photocathode	P.R ($\mu A/1$)	Q.E. At 400mm	Comments
70 52 005	12/15/70	MgF_2	Bi	0		leak in glass seal
70 52 009	12/18/70	MgF_2	Bi	8		
71 04 001	1/5/71	Glass	Bi	50	15.2%	After getting 22 $\mu A/1$ After baking 100° 44 $\mu A/L$
71 04 019	1/21/71	MgF_2	Bi	22		
71 04 025	1/28/71	MgF_2	Bi	19		
71 08 003	2/5/71	MgF_2	Bi	17		
71 08 011	2/19/71	MgF_2	Bi	7.6		
71 13 001	3/3/71	MgF_2	Bi	7.5	4.4 at 420mm	Cr. on faceplate 79% transm.
71 13 005	3/19/71	MgF_2	Bi	0.6		Cr on faceplate
71 13 007	3/23/71	MgF_2	Bi	6/4		
71 13 009	3/23/71	MgF_2	Bi			Internal electrical leakage is not measured
71 13 012	3/26/71	MgF_2/gold	Bi	0		Leak in faceplate due to baking at 400°C
71 13 014	3/29/71	MgF_2	Bi			Faceplate immersed in acid and water. Bright dipped - washed in Alconex

TABLE III (continued)

No.	Date	Faceplate	Photocathode	PR ($\mu A/l$)	Q.E. At 400mm	Comments
71 17 001	4/2/71	Glass	Bi	40		
71 17 002	4/2/71	MgF_2	Bi	0.2		10% chrom. glow discharge
71 17 003	4/2/71	MgF_2	Bi	14		
71 17 004	4/5/71	MgF_2	Bi	12		glow discharge
71 17 004A	4/7/71	MgF_2	Bi	17		glow discharge
71 17 009	4/14/71	MgF_2	Bi	36	8.6%	

TABLE IV

WX-31718

Tube No.	Face-Plate	Photo Surface	P/R White	Environmental Testing	Reticle	Remarks
WX-31222				Shock & Vibration		Shock 8.5 lms. (Target Mesh Touch)
WX-31222				Shock & Vibration		10g. (100-150 Hz) axial, 5g(5-150,350-500) lateral
WX-31222				Shock & Vibration		
5419B	Glass	S-20				
6912-11	Glass	Bi	49	-		Heavy gold raster
70-01-07	MgF_2/Silver	Bi	30	Thermal Shocked		Hazy
70-01-09	MgF_2/Silver	Bi	26	-		Gassy, small leak, tube lost
70-02-02	MgF_2/Silver	Bi	33-0.1 10 Days	Vibration		6g (1000-1500 Hz) gassy, tiny leak, tube lost
70-02-03	MgF_2/Silver	Bi	10	-		Delivered (Res 900-1000 G-90, C-2000 pF)
70-02-06	MgF2/Silver	Bi	20	-		Leak, patched, but tube lost
70-03-01	Glass	Bi	63			(Res=1000) Delivered
70-08-01	MgF_2/430 St. Steel	Bi				Crack faceplate and envelope during Heliarc
70-08-17	MgF_2/gold Carpenter	Bi	22	Shocked and Vibrated not evacuated		Small leak in shoulder pin, resealed and exhausted, checked for 41 days, leak tight.

TABLE IV (continued)

Tube No.	Face-Plate	Photo Surface	P/R White	Environmental Testing	Reticle	Remarks
70-09-20	MgF_2/Gold Kovar	Bi	14	Vibrated, thermal shocked, radial accelerated 35g		Observed for 17 days for leaks, good vacuum. Smoother gold oil, better welding due to Kovar
70-11-05	MgF_2/430 St.Steel	Bi				Crack during Heliarc with improved heat sink
70-10-11	MgF_2/gold	Bi	8	Vibrated, thermal shocked, radial acceleration 35g		Window flange cleaned by baking in reducing atmosphere
71-04-017	Glass	S-20	165			Moly target, strong S-distortion, opened
71-08-005	Glass	S-20	138			Moly target, strong S-distortion, delivered
71-08-010	Monoscope	-				Flat target, not exactly equal to the actual tube
71-26-013	MgF_2/gold	Bi	9.8			Stepless moly target support, less S-distortion, delivered
71-26-020	MgF_2/gold	Bi	12/25 After Bake		AL-Pattern	Stepless (Kovar) target support less S-distortior target broke, delivered
71-30-006	Monoscope	-				0.001 inch limiting aperture in gun structure
71-39-070	MgF_2/gold	Bi	24/13-16		Al-oxide	R-1200,65%/500 G=70 C_{peak}=350/350 nA
71-39-071	MgF_2/gold	Bi	12/11		Al-oxide	Res=1200, 50%/500
71-39-072	MgF_2/gold	Bi		Air		
71-39-127	MgF_2/gold	Bi	18(14/12)		Cr-oxide	Res=1100, 58%/500
71-39-129	MgF_2/gold	Bi	1(14)		Chromium	Loose particle, Res=1200, 60%/500
71-39-134	MgF_2/gold	Bi	10.5		Chromium	Res=950, 32%/500

2.4 Tube Fabrication

Following the adoption of the ruggedized version of the WX-5419B as the basic design for the WX-31718, four areas of the design were identified for modification. These were the faceplate assembly, the image section accelerator electrodes, the target mesh assembly with its supporting structure, and the gun light shield.

The design and fabrication of the face-plate assembly have been described in a previous paragraph and the design finally adopted is illustrated in Figure 3.

The image section accelerator rings were designed as hollow, round structures so that no sharp corners or edges were present. However, difficulties in fabricating these rings to a sufficiently tight tolerance necessitated returning to the simpler "L" shaped form which proved to be entirely adequate. An extremely rigid connection to the contact buttons was found, in practice, to be too rigid and did not allow for expansion and contraction and, in some cases, resulted in breaking of the welds. The less rigid "L" supports were found to provide a more flexible joint, but one which was still strong enough to withstand shock and vibration. All of these parts were carefully electro-polished in order to avoid burrs and rough spots.

The target mesh assembly was a major area of concern. In order to reduce microphonics and resonances of the target substrate, a target ring with a square opening of 1" x 1" was designed. Also, this ring was stiffened by an elevated square rim onto which the substrate was attached. The target support ring was manufactured from Kovar, a material which matches the expansion of the substrate material (aluminum oxide). Other materials which might be used are molybdenum and glass. The use of glass as a target support was investigated and found to be feasible. The aluminum oxide substrate was found to adhere to the glass support and the complete assembly was found to satisfactorily withstand the baking cycle. In all, a total of four such experimental glass target support assemblies were built and tested. However, this effort was not followed through because of lack of time and funds, and a Kovar supporting ring was used throughout the program. In Figure 4, the details of this first Kovar target-mesh assembly are shown. The field mesh supporting ring is made fron inconel, a non-magnetic material. This design proved to be very good mechanically, but electrically it caused some distortions. It was found that the step in the elevated edge of the target caused an electric field distortion in cases where high mesh voltages of several hundreds of volts were applied, and also thick extension of the magnetic Kovar rim in the direction of the magnetic field lines caused a distortion in the magnetic focus field. This assembly was redesigned as shown in Figure 5 and the new design used in the final tubes. In the new design, the target support ring is still manufactured from Kovar. It should be mentioned that attaining a distortion free performance depends not only on the tube, but also upon the focus and deflection coil systems used. Therefore, a distortion free performance should be understood only in this context. In the final tubes there was still some residual distortion, the cause of which will be discussed in the later paragraph.

The gun design was similar to that used in the ruggedized version of the WX-54198 (the WX-31222) with the exception that a light shield was added. This shield consists of a metal cylinder enclosing two ceramic wafers which support the cathode heater assembly. The metal cylinder has three feed throughs in the form of eyelets for the cathode and the tube heater connections. It was found that this design satisfactorily shielded light from the cathode and heater.

FIRST TARGET MESH ASSEMBLY

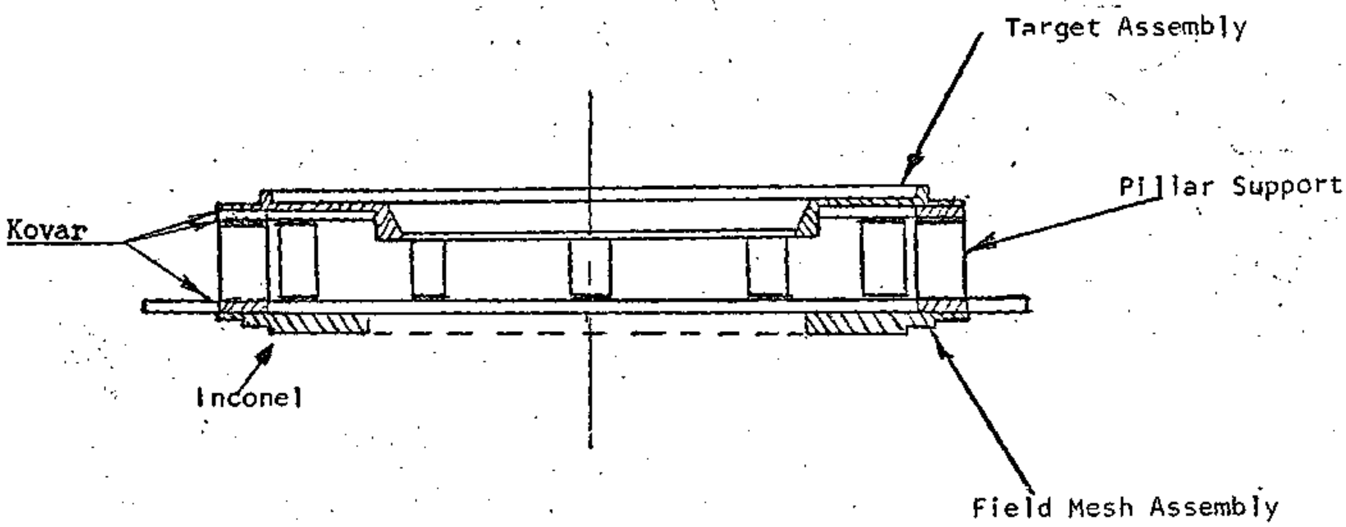

Figure 4

REVISED DESIGN OF THE TARGET MESH ASSEMBLY

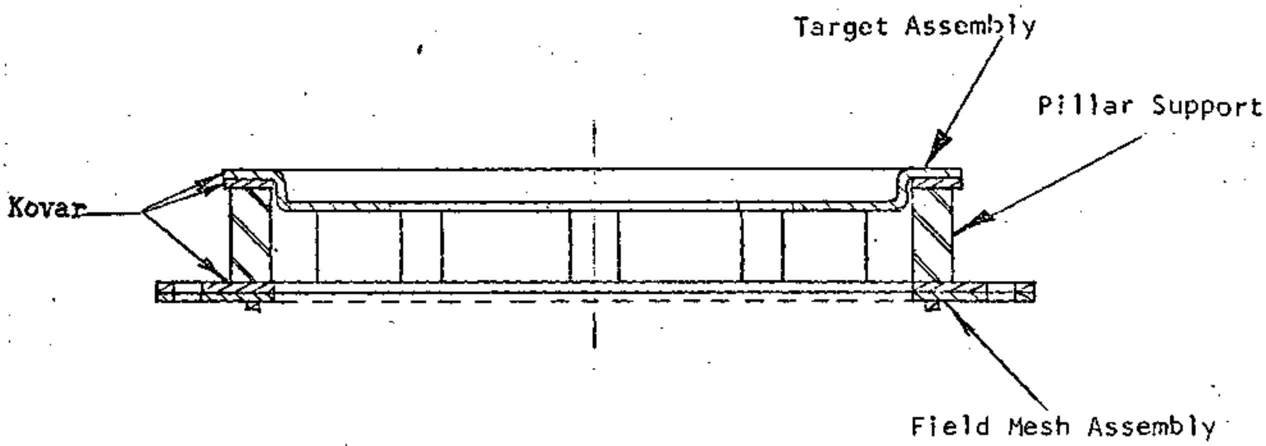

Figure 5

A beam defining limiting aperture of 0.0018 inch was used in the first design. This was reduced later to 0.001 inch and, finally, to 0.0006 inch. The smaller apertures increased the resolution of the tube significantly, but only at the expense of reducing the available reading beam current. This, however, is not a disadvantage in the slow scan application for which this tube is intended. For the smaller paerture, a change in the G-2 spacing was made to correct for the change in cut-off voltage. Table 4 summarizes all the tubes built. In addition to the tubes made with a bi-alkali photosurface, two tubes were also made with an S-20 photocathode.

In order to study the performance of the reading gun, two monoscope tubes with a metal disk positioned in place of the target were manufactured. The target metal disk was composed of the original target support which is Kovar and the non-magnetic metal disk insert made from inconel, so that the magnetic properties were the same as those of the actual target. The target mesh assembly was exactly like those used in the actual tube. The inconel disk was painted with liquid bright platinum and heated in a furnace to approximately 450°C. Onto the platinized surface were now attached a metal face mask etched with the Air Force test pattern in each corner and the center and connecting lines between the patterns. Through this mask, chromium was evaporated, so that a chromium pattern appeared on the platinum layer. Both metals have a different work function which creates different contact potentials and, therefore, the beam acceptance is different for both metals. This allows studies at very low target voltages of only a part of one volt. At higher target voltages another physical phenononen will take over, the different secondary emission capability of both metals. The second effect reverses the image appearance in the case of platinum and chromium and there is a target voltage range, where both affects cancel each other out.

Finally, the last six tubes were provided with a reticle pattern on the inside of the faceplate in order to provide a reference for measurement and orientation purposes. The reticle was made by a metal evaporation consisting of short right angle lines in the four corners of the picture. There were used two different metals, aluminum and chromium. For cleaning purposes of the window there was applied a short glow discharge in a slight oxygen atmosphere. This oxidized slightly the reticles and by some sputtering effect the image of the reticles was widened by a bright rim around the dark reticle. This was especially pronounced with aluminum. The bright rim appearance was caused by an enhanced photoresponse where a thin metal oxide layer was located under the photoemissive surface. The cleanest reticles were achieved with chromium.

2.5 Environmental Testing

Four types of environmental testing were conducted. These were shock, sinusoidal vibration, thermal cycling and radial acceleration.

Before the final design work began, three tubes of a design similar to the WX-31718 and of a ruggedized construction (WX-31222) were shock and vibration tested. The first of these three tubes underwent a shock of 8.5 g's for a duration of 11 milli-seconds. A small crack, with some loss of KCl occurred at the rim of the target adjacent to the target ring. The other two tubes were subjected to a vibration of up to 10 g's at frequencies between 100 and 150 Hz in the direction of the longitudinal axis at 5 gs at frequencies between 5 to 150 Hz and 350 to 550 Hz in the lateral direction. Both tubes experienced target to suppressor mesh touches, but otherwise were not affected. These tests indicated that the mechanical design of the WX-31222 was satisfactory, but that a tube could not survive with a closely spaced suppressor mesh. In order to investigate the possibility of building a tube of this kind, but without a suppressor mesh, it was decided to build a WX-5419B without a mesh and test it for microphonics. This was done and the microphonics were found to be drastically reduced, and it was decided for this, and other reasons, to adopt a design without a suppressor mesh. All of the following tests summarized below were conducted with the new suppressor meshless design.

Thermal Cycling: Three tubes were exposed to this test. No. 70-01-07 with a silver chloride seal was exposed five times to -55°C for approximately one hour and in between warmed up to +25°C, also for at least one hour. No damage resulted. No. 70-09-20 and No. 70-10-11 with a gold foil seal were exposed to the same treatment. No damage resulted. The last two were inspected operationally; the first was measured with respect to photoresponse and gas content only.

Vibration: Five tubes were exposed to vibration testing. Two of these: No. 70-01-07 and 70-02-02, with a silver chloride seal were vibrated during operation in order to observe details on the monitor. However, for technical imperfections the pictures were not sharply focused, but one could observe resonances very well. The tubes were vibrated in two directions, longitudinally and laterally.

The first tube was tested in a frequency range of 24 to 2000 Hz. The acceleration level was 12.5g to a frequency of 110 Hz, and 4 g to a frequency of 2000 Hz. There could be observed many resonances and it seems that they contribute to the loosening of particles, especially at the higher frequencies. Cautiously, one could say that the target surface withstood a g level of 10g at the low frequency range to 110 Hz and 3g for the upper frequency range. The second tube, No. 70-02-02, was tested with 10g in the low frequency range, to 110 Hz and with 7.5g in the high frequency range in the longitudinal direction. For the lateral direction the equipment allowed 7.5g till 1000 Hz, 6g till 1500 Hz and 5g till 2000 Hz. The resonance frequencies were recorded and some photographed at different g levels. The standing waves were far more pronounced at higher g levels and the nodes and antinodes are closer together at the higher frequency range, so that the bending radius is smaller. This seems to be in accordance with the finding that the target generally withstands a higher g level at the lower frequency range. From this tube it can be said that the target withstood 10g safely till 110 Hz. In the range till 1000 Hz and at 7.5g some particles came loose. In the frequency range from 1000-2000 Hz, an acceleration of 5g seems safe, whereas at 7.5g and 6g respectively, very many spots appeared.

The tubes No. 70-09-20 and 70-10-11 were tubes with the gold foil sealing technique. The first of these two tubes was tested so that a low g level of 2 g for the entire frequency range to 2000 Hz was imposed and the target was afterwards photographed in operation. The 2g level did not cause any change in the target appearance. The next level was 5g till a frequency of 110 Hz and 3.5g till a frequency of 2000 Hz; also here no change in appearance could be observed. The third level was between 10g and 14g for the low frequency range and 7.5g for the high frequency range. Here one could now observe quite a few spots on the target. The second tube was tested at the same levels but not at the 2g level, because it was clear that at this level the target stays unchanged. However, the other two levels were run twice; once with a charge corresponding to 15 volts on the target and after that with the discharged target. Here one could observe a visible increase in the number of spots at the 12g level in the low frequency range when the target was discharged. At the high frequency, a larger number of spots appeared at the 7.5g level and a change for the charged and noncharged condition could not be observed. Both tests indicated that these two target withstood 10g safely in the lower frequency range and 4-5 g in the upper range.

Tube No. 70-08-17 also with a faceplate built by the gold foil technique, was vibrated with no vacuum to simulate the pressure condition of outer space. No visible damage occurred and no leak could be detected by a leak detector.

Radial Acceleration Testing: Two tubes of the gold foil technique type No. 70-09-20 and No. 70-10-11, were subjected to a radial acceleration of 35g for 4 minutes with acceleration force directed so as to pull the faceplate assembly away from the tube body. The radial arm has a diameter of 10 feet. Both tubes were tested operational before and after the acceleration. No damage occured and the target appearance was unchanged.

Shock: Tube No. 70-09-20 was shocked at two different levels, 15g and 50g. The tube withstood both shocks; the target did not change its appearance. Tube No. 70-08-17 was shocked at 15g under conditions of no vacuum. No visible damage occured and no leak could be detected by a leak detector.

2.6 Ultra-Violet Spectral Response

The WX-31718 has been designed for operation in the short ultra-violet region of the spectrum. Since improper treatment of the entrance faceplate can easily reduce its transmittance, it was, therefore, considered desirable to measure the spectral response as far as 1150 angstroms at which wave-length the transmittance of the magnesium flouride crystals begins to sharply decline. A Spex 3/4m UV vacuum spectrometer, type #1500 was used for these measurements. The wave length of the spectrometer was calibrated first with a Penn Ray mercury lamp and also with respect to some known peaks of the hydrogen spectrum. The intensity measurements were done, by comparison, with a standard image tube which was calibrated by NASA Goddard Space Flight Center. This tube was equipped with a magnesium fluoride window and a CsTe photosurface. The calibrated spectral range was from 1160 angstroms to 3400 angstroms. A sodium salicylate screen on a glass plate in conjunction with the photo-multiplier was also used. The light source includes a hydrogen gas discharge lamp which can be used also with other gasses such as crypton. The results of the measurements are shown in Figures 6 to 10. It can be said that generally the quantum efficiency in the ultra-violet region was related to the white light photoresponse measured in a 2859°K white source. Some problems with the UV spectrometer prevented the measurements from extending beyond the wave length of 1400 angstroms; a leak in the water jacket of the hydrogen lamp was found and also the grating and the mirrors were contaminated with oil. After cleaning and recalibration it is intended to repeat these measurements to wave lengths down to 1150 angstroms.

3.0 SUGGESTIONS FOR FURTHER DESIGN IMPROVEMENTS

The present tube shows a small deviation from unity magnification. This is caused by an electro-static lens created by the last image section accelerator ring and the anode ring. The potential of the last accelerator ring penetrates deeply into the anode ring space causing there, a magnification and the magnetic field causes in turn, a rotation of the image which is manifested by a severe S-distortion in the corners of the target. Some improvement can be achieved by not connecting the anode ring to the ground, but by using it as the last accelerator ring. It should be mentioned here, that this S-distortion should not be confused with the S-distortion generated by the reading section. For an improved version of the tube, the anode ring should be redesigned. In this case, a design with a second lower metal flange in the image section would be advisable which would also allow a much simpler mounting procedure.

The second area of possible improvement is the gun. The small limiting aperture of 0.0006 inches has caused a remarkable improvement in the resolution. However, this was achieved by sacrificing the available reading current. In the intended application, this is permissible, however, in some applications it might be necessary to employ higher currents. The efficiency of the gun can be improved only if the aberration of the gun is reduced which means, mainly, shortening the cross-over line into a cross-over point at the plane of the limiting aperture. This would require an electron optical systemwith a spherical cathode.

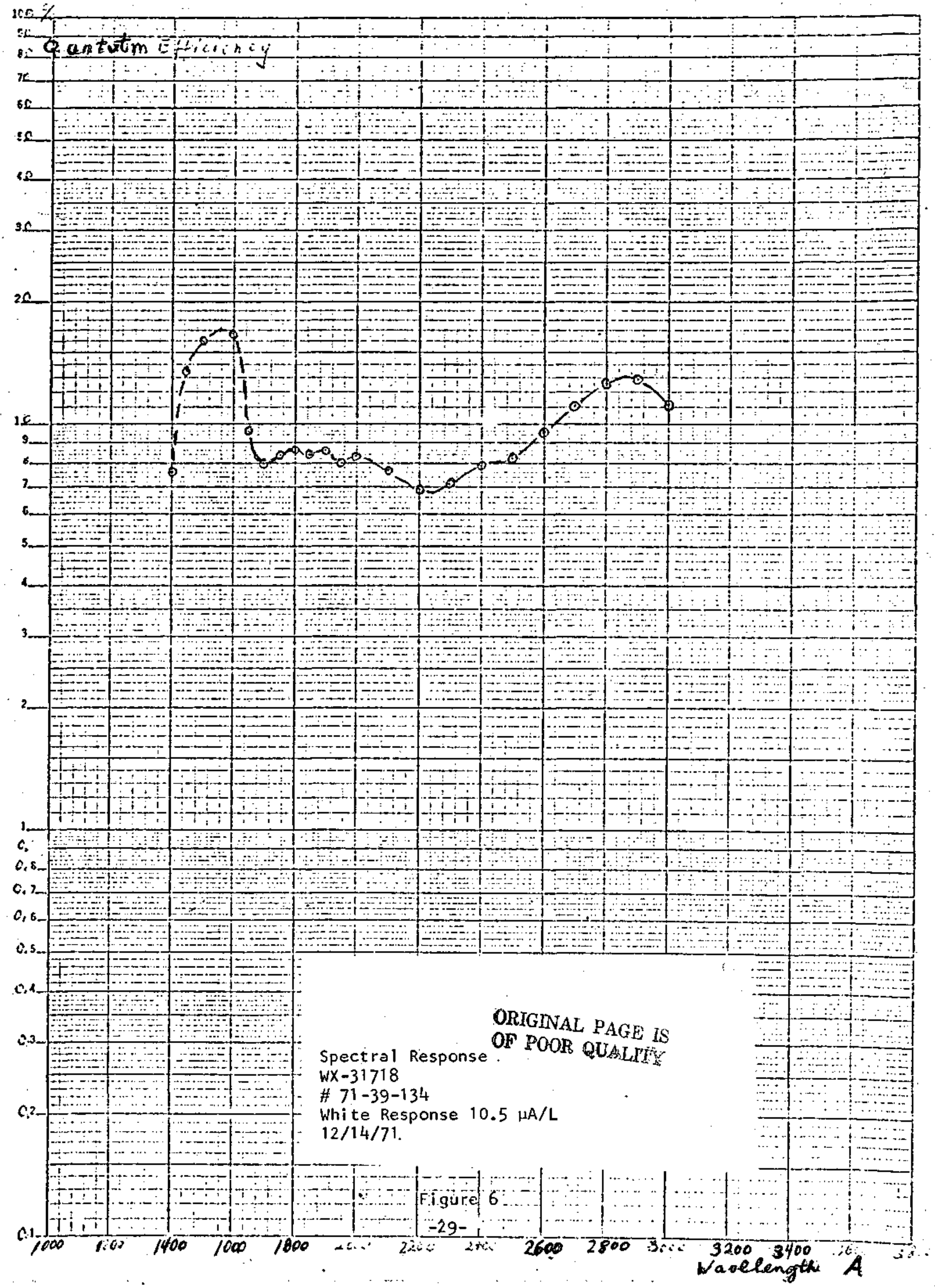

ORIGINAL PAGE IS OF POOR QUALITY

Spectral Response
WX-31718
71-39-134
White Response 10.5 µA/L
12/14/71

Figure 6

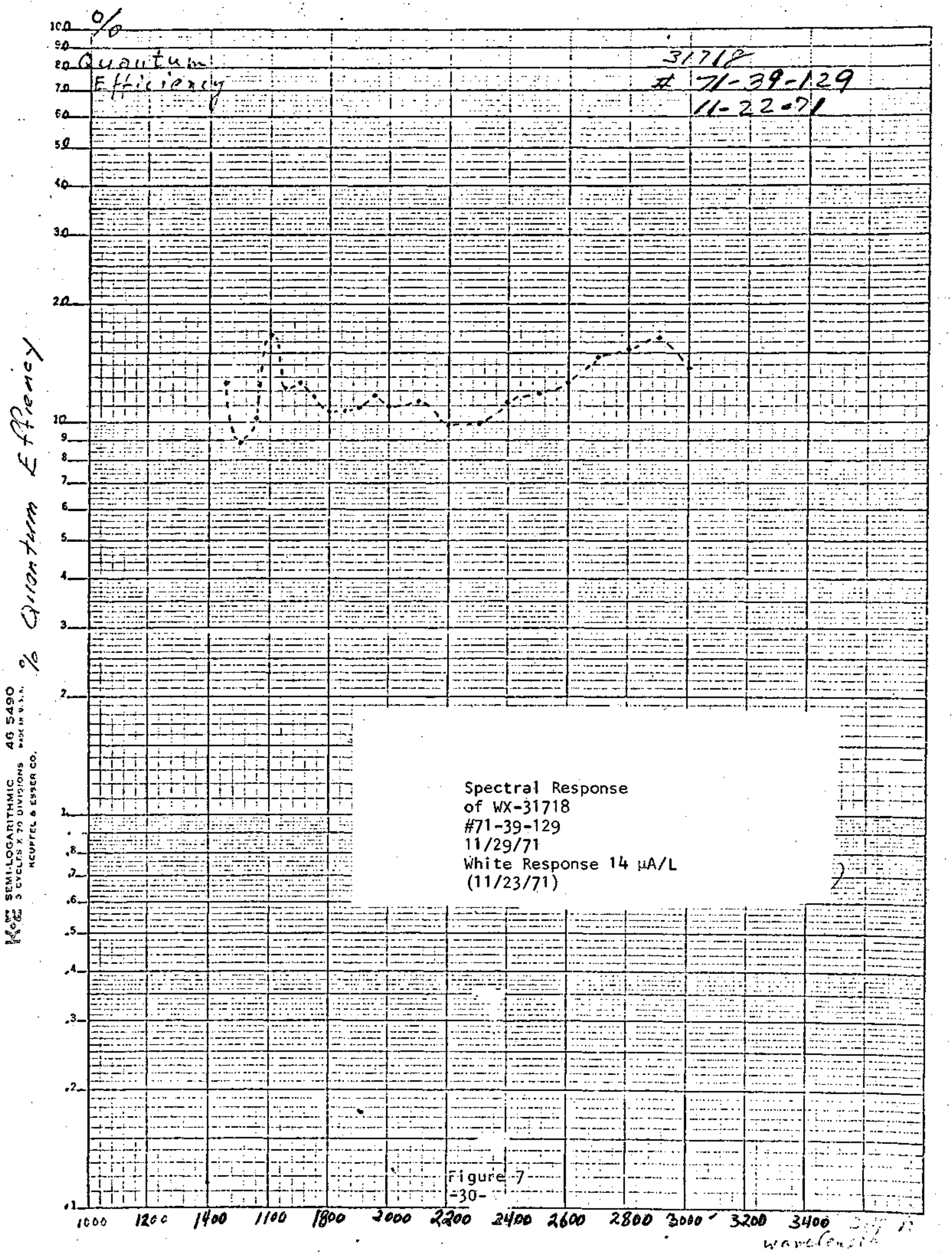

Spectral Response
of WX-31718
#71-39-129
11/29/71
White Response 14 µA/L
(11/23/71)

Figure 7

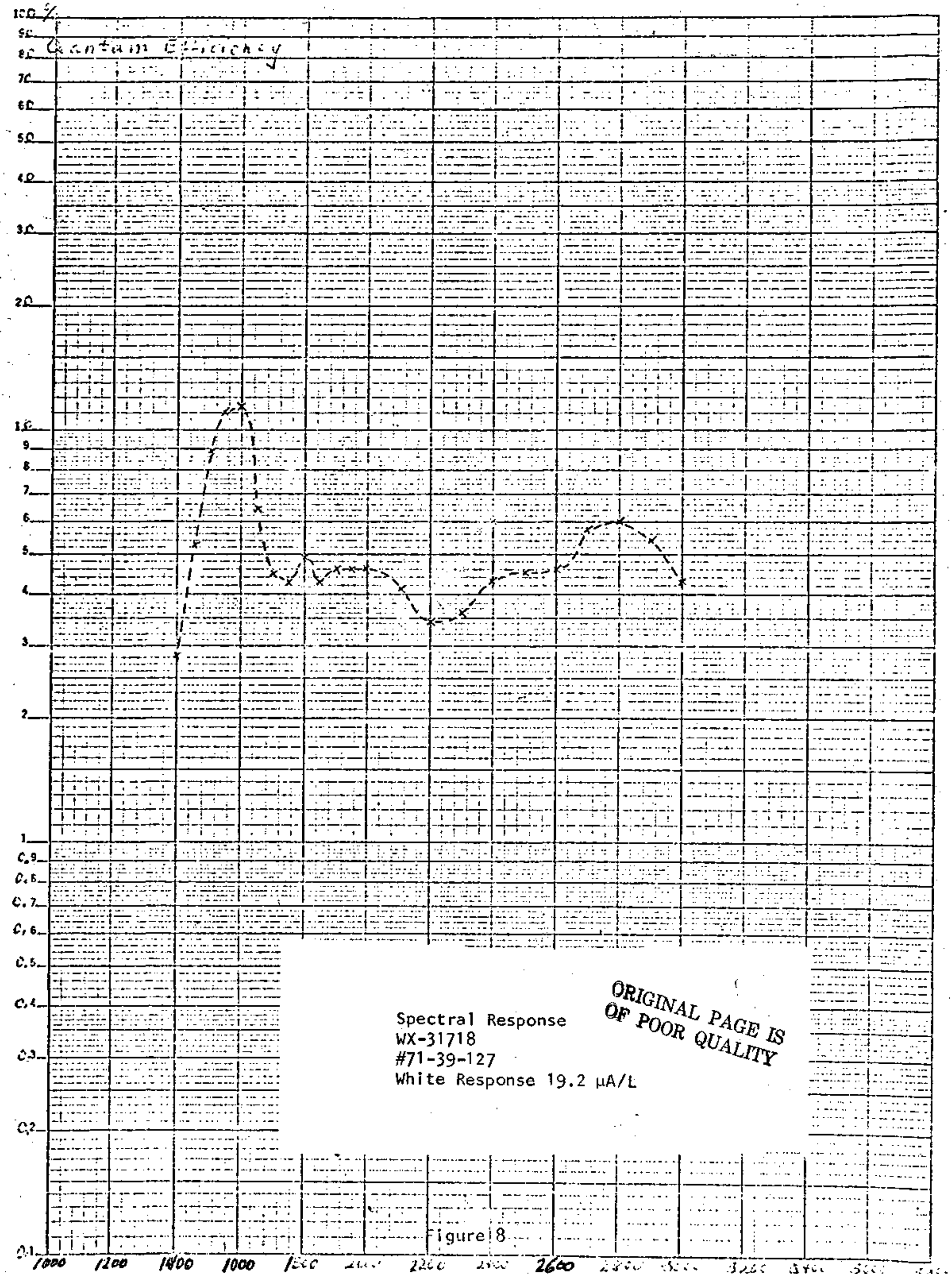

Quantum Efficiency
Spectral Response
WX-31718
#71-39-127
White Response 19.2 μA/L
Wavelength A
K&E SEMI-LOGARITHMIC 46 5490
3 CYCLES X 70 DIVISIONS MADE IN U.S.A.
KEUFFEL & ESSER CO.

Figure 8

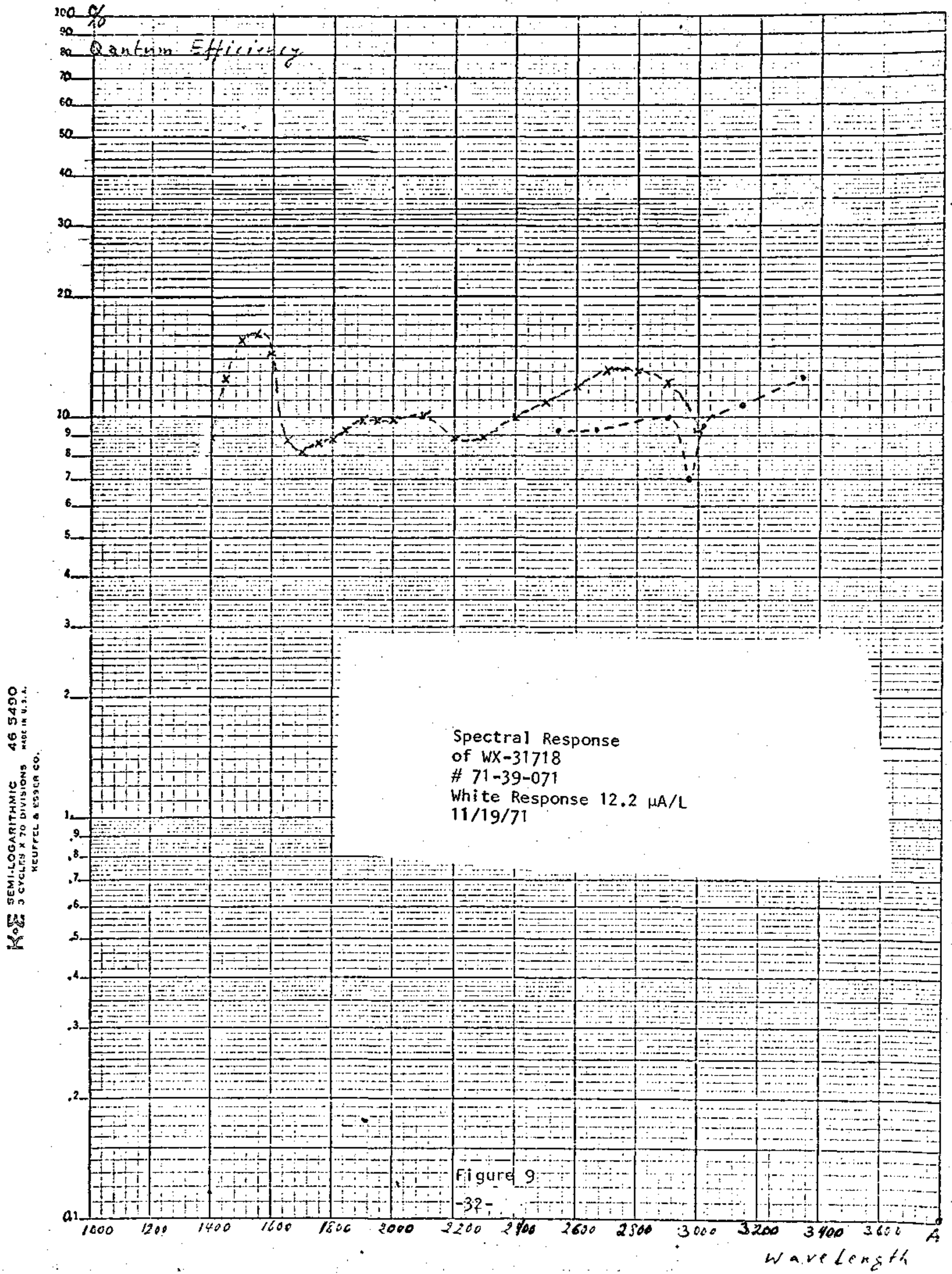

Spectral Response
of WX-31718
71-39-071
White Response 12.2 μA/L
11/19/71

Figure 9

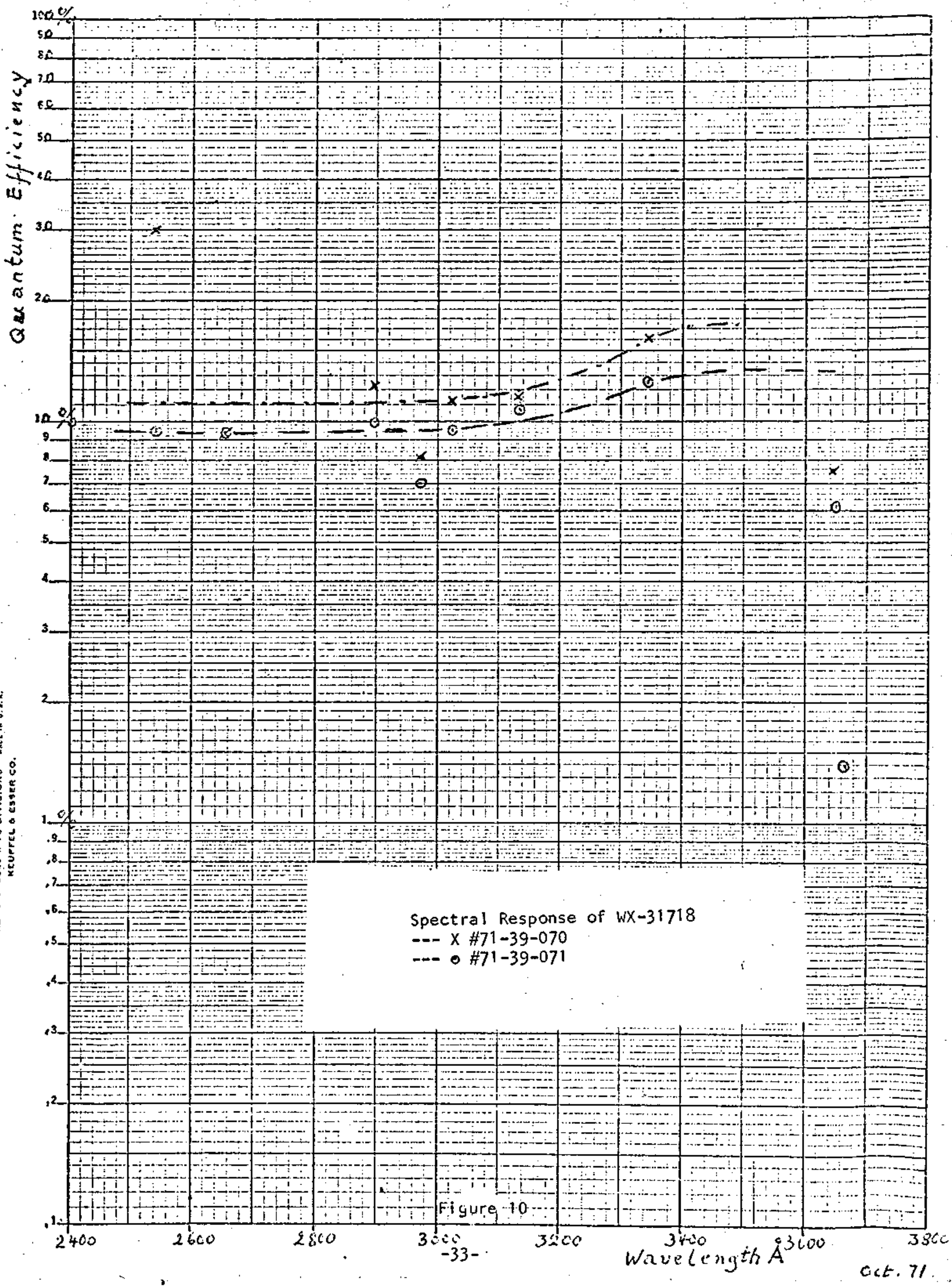

Quantum Efficiency
100%
90
80
70
60
50
40
30
20
10 %
9
8
7
6
5
4
3
2
1 %
.9
.8
.7
.6
.5
.4
.3
.2
.1
2400
2600
2800
3000
3200
3400
3600
3800
Wavelength Å
Spectral Response of WX-31718
--- X #71-39-070
--- ⊙ #71-39-071
K+E SEMI-LOGARITHMIC 46 5490
3 CYCLES X 70 DIVISIONS MADE IN U.S.A.
KEUFFEL & ESSER CO.
Oct. 71

Figure 10

APPENDIX 1

AN INVESTIGATION OF THE INFLUENCE OF NON-PARALLELISM OF THE PHOTOCATHODE AND TARGET ON THE RESOLUTION IN MAGNETICALLY FOCUSED IMAGE TUBES

AN INVESTIGATION OF THE INFLUENCE OF NON-PARALLELISM OF THE PHOTOCATHODE AND TARGET ON THE RESOLUTION IN MAGNETICALLY FOCUSSED IMAGE TUBES

This investigation is conducted to get a rough feeling how much tilting of the faceplate against the target can be allowed in the manufacture in order to maintain a reasonable edge resolution. We did not try to resolve this problem so far as to calculate the transfer function because this would require an extended effort in time, but calculated the radius, a, of the disk of confusion for an electron leaving the photocathode under an angle of 90° against the normal and with an initial velocity of one electron volt. This will be the most unfavorable condition in the violet part of the visible spectrum. For the UV of 2000 Å the initial velocity may go up to 2 eV and for 1500 Å to 6 eV. The radius of confusion, a, will be affected by the square root of the factor of increase in voltage. (See equation 2.) and 3.))

To get a measure for the resolution, we have chosen a bar width of the radius of confusion. This will certainly not be the limiting resolution but much higher in contrast, so we will have a safety factor of maybe 2 for the higher initial velocity of electrons released by shorter wavelength in the UV region.

Our calculation is based on a uniform magnetic field strength, H, directed parallel to the tube axis, z. The electric field, E, is also directed parallel to the tube axis, and is considered constant over the entire tube diameter in case I. So in the equation for the field strength $E = \frac{V}{d}$, the distance, d, is taken constant and equal to the focal length. Since this is not correct, we have chosen a Case II where the field strength is constant only over the small area of the electron ray pencil leaving one spot of the photocathode, however, varies from spot to spot accordingly to the tilting and the actual distance, Z_φ, of this spot from the target. This means that d equals Z_φ. Also this case does not agree fully with the reality. The true appearance might be anywhere inbetween. By the tilting of the two planes the electric field will bend a bit, which we neglected as small. Furthermore, the influence of the tilted field may be only in a small region near the target with little influence on the focal length. So we believe the true result will be somewhere between the two considered cases.

In the following we gather a few equations we have used in the computation of the attached table.

1.) $r = 3.376 \frac{\sqrt{V_o}}{H} \sin\alpha$

r = Radius of the spiraling electron in (cm)

V_o = Initial velocity of electrons leaving the cathode under angle α to the normal in (Volt)

H = Magnetic field strength in (Gauss)

2.) $a = 6.75283 \frac{\sqrt{V_o}\sin\alpha}{H} \sin\left[\frac{0.2965\, H d \sqrt{V_o}\cos\alpha}{V}\left(\sqrt{1+\frac{V\, Z_p}{d\, V_o \cos^2\alpha}}-1\right)\right]$

a = Radius of disk of confusion in (cm)

d = Distance, target to photo cathode at center in (cm)

V = Photocathode Voltage in (Volt)

Z_p = Actual distance photocathode to target of considered spot in (cm)

3.) $a = 6.75283 \frac{\sqrt{V_o}\sin\alpha}{H} \sin\frac{\varphi}{2}$

φ = Total angle of spiral (2π for focus)

4.) $Z_p = 5.6938\left(\frac{V}{2d\,H^2}\varphi^2 + \frac{0.593\sqrt{V_o}\cos\alpha}{H}\varphi\right)$

In Case II we set $d = Z_p$

5.) $\varphi = 2 \arcsin\frac{a}{2r} = 0.593\, H\sqrt{\frac{d}{V} Z_p}$

We computed the magnitude of the disk of confusion, resolution figures and the location Z_p of the image dependent on the angle of rotation φ. The results are put together in the attached table and a graph. We used for V = 8000 Volt, H = 80 Gauss, Vo = 1 Volt, $\alpha = 90°$ and in Case I, d = 11.85 cm.

In Column I of the table is given half the angle of rotation in radians of the spiraling electron leaving the cathode under 90° and an initial velocity of one eV. So $\frac{\varphi}{2} = 1.0\pi$ is the exact focus point for that specific electron. The next column is the radius of the disk of confusion caused by defocussing. Column three is a resolution value in line pairs per mm so that the line width is chosen equally to the magnetude, a. This resolution value will certainly exhibit a much higher contrast than generally connected with the limiting resolution. We have not tried to go into this calculation because major time efforts are then necessary. Column 4 are the corresponding values of the resolution rearranged in TV lines per inch picture weight. Columns 5 and 7 are the target distance corresponding to the rotation angle $\frac{\varphi}{2}$. Columns 6 and 8 are the distance difference Δz_y in mm, referred to the focal length (row 8). In column 8 the defocussing effect is symmetrical to the focal length, whereas in column 6, this is not the case.

From the graph, one can draw the conclusion a tilting of 0.5 to 1.0 mm over the total faceplate diameter of 50 mm will give a good distinguishable contrast for 70 to 80 line pairs per mm, which corresponds to 3500 - 4000 TV lines per one inch picture height. This will impair the overall contrast function not to a great extent.

Table.

				Case I		Case II		
$\frac{\varphi}{2}$	a [cm]	$R=\frac{0.1}{2a}\left[\frac{LP}{mm}\right]$	$R\cdot 50.8\left[\frac{TVL}{inch}\right]$	$Z_\varphi=\left(\frac{\varphi}{2\times0.912}\right)^2$ [cm]	ΔZ_φ [mm]	$Z_\varphi=\frac{\varphi}{2\times0.2652}$ [cm]	ΔZ_φ [mm]	
0.96 π	0.010582	4.7251	240.1	10.9177	− 9.288	11.3723	− 4.738	1
0.97 π	0.007940	6.2975	319.9	11.1463	− 7.001	11.4907	− 3.554	2
0.98 π	0.005301	9.4322	479.1	11.3773	− 4.691	11.6092	− 2.369	3
0.99 π	0.002652	18.8525	957.7	11.6108	− 2.357	11.7277	− 1.185	4
0.995 π	0.001325	37.7301	1916.7	11.7283	− 1.182	11.7869	− 0.592	5
0.997 π	0.0007892	63.3553	3218.4	11.7755	− 0.7097	11.8106	− 0.355	6
0.998 π	0.0005284	94.6253	4807	11.7991	− 0.4734	11.8224	− 0.237	7
1.000 π	0.0000	∞	∞	11.8465	0.000	11.8461	0.000	8
1.002 π	0.0005284	94.6253	4807	11.8939	0.4743	11.8698	0.237	9
1.003 π	0.0007892	63.3553	3218.4	11.9177	0.7118	11.8817	0.355	10
1.005 π	0.001325	37.7301	1916.7	11.9652	1.188	11.9054	0.592	11
1.01 π	0.002652	18.8525	957.7	12.0846	2.381	11.9646	1.185	12
1.02 π	0.005301	9.4322	479.1	12.3251	4.786	12.0831	2.369	13
1.03 π	0.007940	6.2975	319.9	12.5679	7.215	12.2015	3.554	14
1.04 π	0.10582	4.7251	240.1	12.8131	9.667	12.3200	4.738	15
1	2	3	4	5	6	7	8	

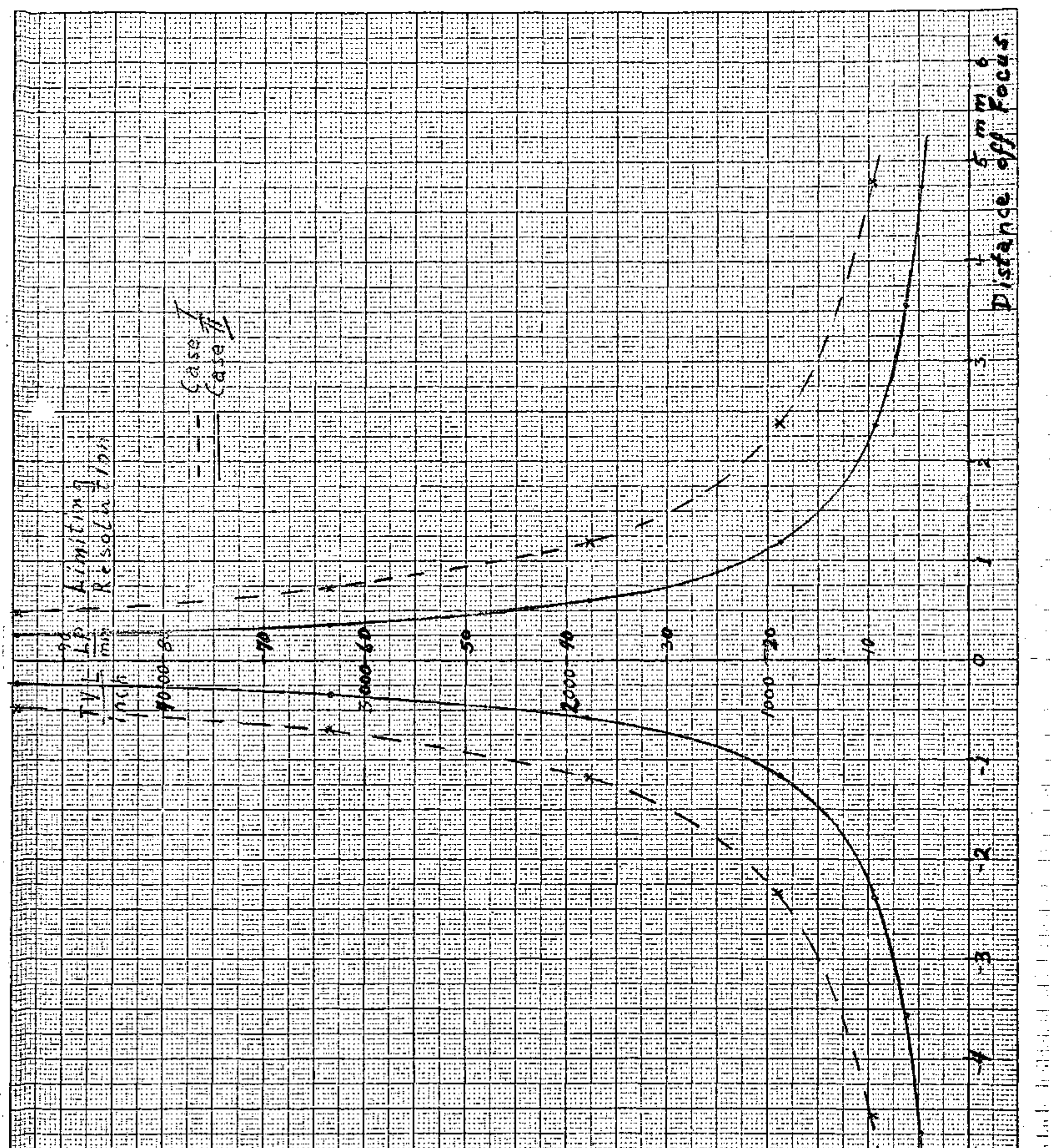
TVL / inch
LP / mm
Limiting Resolution
Case I
Case II
Distance off Focus mm
10000
5000
2000
1000
70
60
50
40
30
20
10
-5
-4
-3
-2
-1
0
1
2
3
4
5
6

APPENDIX II

CALCULATION OF THE SQUARE WAVE RESPONSE OF A MAGNETICALLY FOCUSSED IMAGE SECTION

CALCULATION OF THE SQUARE WAVE RESPONSE OF A MAGNETICALLY FOCUSSED IMAGE SECTION

It is assumed that the magnetic as well as the electric field lines are uniform and parallel to the tube axis. Therefore there is only a need to consider a single point of the photocathode; its size should be negligibly small compared to the dimensions of the disk of confusion.

It is furthermore assumed that electrons leave the said point in all directions and the intensity distribution in these directions may follow a cosine law, which assumption is justified by similar behavior in secondary emission.

It is furthermore assumed that the initial velocity distribution of the emitted electrons follows a sine square function. This assumption is based on energy distribution curves published in "Handbuch der Physik, Encyclopedia of Physics, Volume 21, pg. 358-359, Publisher: Springer" and in "Tabellen der Elektronen-physik, Jonenphysik und Uebermikroskopie, by Manfred V. Ardenne, Volume 1, Deutscher Verlag der Wissenschaften, pg. 91-92." This assumption is more correct for small maximal energies than for larger. However, it will give a fairly accurate response curve. To employ an actual measured curve and integrate it would have been more time consuming and would not have yielded greater accuracy, because these measured curves depend highly upon conditions and are not easy to take accurately.

The computation is made in two parts. First, there is calculated the electron density distribution over the circle of confusion and, secondly, there is calculated how intense the overlapping circles of confusion brighten the black bars of an alternate row of black and white bars of infinite number and infinite extension.

In order to calculate the density distribution, one has just to compute the radius a of the disk of confusion dependent upon the magnetic field strength H, the accelerating voltage V, the initial velocity of the electrons in eV_o, the length of the tube and the starting angle α of the electrons. The radius, a, is then, using the units Volt, Gauss, cm:

$$1) \quad a = 6.75283 \frac{\sqrt{V_o}}{H} \sin\alpha \sin\left[0.29648 \frac{Hd}{\sqrt{V}}\left(\sqrt{1+\frac{V_o}{V}\cos^2\alpha} - \sqrt{\frac{V_o}{V}}\cos\alpha\right)\right]$$

True focus, which means a = 0, is achieved if the magnitude under the bracket becomes an integer multiple of π. This delivers an equation for the solution of the length of the tube. However, this definition equation is multivalued, dependent upon the magnitude of $\frac{V_o}{V} \cdot \cos^2\alpha$. This value is small and we will choose its value zero for the focal length, which means that those electrons leaving the photocathode under the angle 90° will be true focussed. We get then as definition equation:

$$2) \quad d = \frac{\pi}{0.29648} \frac{\sqrt{V}}{H} \qquad \text{(cm)}$$

For V = 8000 volts and H = 80 Gauss, we get d = 11.85 cm.

Equation 1) gives us the answer at which distance from the center point at the target an electron leaving the cathode under the angle α and an initial energy corresponding to V_o electron volts will be found. Now we have said that we assume a cosine distribution of the number of electrons leaving the photocathode. So the density distribution at the target will be:

3) $D = \frac{C}{2a} \cdot \cos\alpha = \frac{C}{2a} \sqrt{1 - \sin^2\alpha}$

To go further we have to simplify equation 1). Introducing 2) into 1) gives:

$$a = 0.08441 \sqrt{V_o} \sin\alpha \sin\left[\pi\left(\sqrt{1 + \frac{V_o}{V}\cos^2\alpha} - \sqrt{\frac{V_o}{V}}\cos\alpha\right)\right]$$

and converting the square root into a series, we get:

4) $a = 0.08441 \sqrt{V_o} \sin\alpha \sin\left[\pi\left(1 + \frac{V_o}{2V}\cos^2\alpha - \sqrt{\frac{V_o}{V}}\cos\alpha\right)\right]$

Approximating the sine function by the first two terms of its series expansion, we get:

5) $a = 2.9648 \cdot 10^{-3} V_o \sin\alpha \cdot \cos\alpha \left(1 - \frac{1}{2}\sqrt{\frac{V_o}{V}}\cos\alpha\right)$

If we now substitute 3) for 5) and solve the equation for D, we get for the density distribution, neglecting again small terms of higher orders:

6) $D = \frac{C}{2a}\left[\sqrt{\frac{1}{2} + \frac{1}{2}\sqrt{1 - \frac{a^2}{K^2 \cdot V_o^2}}} + \sqrt{\frac{1}{2} - \frac{1}{2}\sqrt{1 - \frac{a^2}{K^2 \cdot V_o^2}}}\right.$

7) Where $2K = \frac{6.75283 \cdot \pi}{H\sqrt{V}}$

Equation 6) describes the density distribution for a fixed initial velocity of the emitted electrons over the entire radius, a, of the disk of confusion. The equation does not describe the real density distribution dependent upon the initial velocity because the density depends upon C in equation 3) which will be different for every initial velocity. We have rather to choose for C a suitable function of V_o and $V_{o\ max}$. A sine square function will not entirely fit the true initial velocity distribution, but will fairly well describe it for not a too large $V_{o\ max}$. Applying this function in 3) and 6), we get:

$$8)\quad D = \frac{\sin^2\left(\frac{\pi V_o}{V_{o\ max.}}\right)}{2\ a}\left[\sqrt{\frac{1}{2}+\frac{1}{2}\sqrt{1-\frac{a^2}{K^2\cdot V_o^{\ 2}}}}+\sqrt{\frac{1}{2}-\frac{1}{2}\sqrt{1-\frac{a^2}{K^2\cdot V_o^{\ 2}}}}\right]$$

Equation 8) has now to be integrated over all initial velocities from $V_o = 0$ to $V_o = V_{o\ max.}$ This is possible only by numerical integration, where the integration has to stop for each selected radius, a, always when $\frac{a^2}{K^2 V_o^{\ 2}} \gtreqless 1$. This summation with an increment ΔV_o is done by equation 9):

$$9)\quad D = \Delta V_o \sum_{V_o=\frac{a}{K}}^{V_{o\ max}} \frac{\sin^2\left(\frac{\pi V_o}{V_{o\ max}}\right)}{2\ a}\left[\sqrt{\frac{1}{2}+\frac{1}{2}\sqrt{1-\frac{a^2}{K^2\ V_o^{\ 2}}}}+\sqrt{\frac{1}{2}-\frac{1}{2}\sqrt{1-\frac{a^2}{K^2\ V_o^{\ 2}}}}\right]$$

The radius of confusion is reached when:

$$10)\quad 1 - \frac{a^2}{K^2\ V_{o\ max}^{\ 2}} = 0$$

A small computer subroutine program was developed to compute equation 9).

In a second part we calculated for a row of alternate black and white stripes, of infinite extension, how much the black stripes in its center were brightened by the overlapping circles of confusion of the white bars. The procedure is described in the report "Catadioptric Image Amplifier" by J. Pietrzyk, Technical Report AFAL-TR-68-317, on pages 43 - 53. The calculations were made in order to compute the contrast transfer function of a square wave for an optical system. We have used equation (2.10) for the calculation of the contrast and equation (2.15) for the brightening of the black stripes and part of the same equation to calculate the 100% white energy level according to page 49 of the reference.

We set up a computer program including the subroutine mentioned above to calculate the contrast versus different stripe width. We made the calculations for an image voltage of 8000 volts and a magnetic field strength of 80 Gauss, asking for the transfer function for three different maximal initial electron velocities corresponding to 1, 2, and 3 electron volts respectively. The results are shown in figures 1 and 2, where figure 1 shows the electron density distribution for the three cases and figure 2 the square wave response.

Figure 1 is self-explanatory and nothing more has to be said. It might be interesting to notice the long tail, which all three curves exhibit very similar to the light distribution in optical systems. To figure 2 there is the following to say. The accuracy is better at the higher contrast values than at the lower values. Thus the long tails may not give an accurate magnitude of the limiting resolution.

Conclusions

The calculations seem generally acceptable. The most questionable assumption is the initial energy distribution of the electrons. I have added to this report copies of the two references on the initial velocity, which may help to get a better feeling for the validity of the calculated curves. Figures 46 and 47 of the first reference and the lower two curves of page 92 of the second reference were considered. Page 91 gives the maximum theoretical initial velocity in volts versus the wavelength of the incident light for various work functions. From his curve one comes to the conclusion that for UV-imaging a photocathode of a high work function, or e.g., a short extended long wave limit, would give a better resolving power because the maximum initial velocity corresponding to $V_{o\ max.}$ is smaller. If one compares the measured curves from the report, "Exploratory Development of High Resolution Television Camera Tubes", October 1966, page 31, which is also attached, with the calculated curves, the measured curve would lie just a little above curve II. The $V_{o\ max.}$ for a tri-alkali photocathode, illuminated with white light, may lie between 1 and 1.5 volts. With this figure, the contrast would lie between the calculated curves II and III, which seems to be a very reasonable comparison;and a basic improvement of the image section is only possible if the factor K in equation 10) becomes smaller, because then also the radius, a, of the disk of confusion becomes smaller. In the definition equation 7) for K, it can become smaller if either the magnetic field strength, H, or the electric field or both are increased. However, one has also to consider equation 2) for the length of the tube. A 10% increase in voltage would require 5% increase in the magnetic field strength in order to keep the length unchanged. This would decrease the magnitude of K and also the radius of the circle of confusion by 16%. This would shift the contrast curves in its upper portion also by approximately 16% to the right.

Joh. Pietzsch

Att: 2 curves
3 references

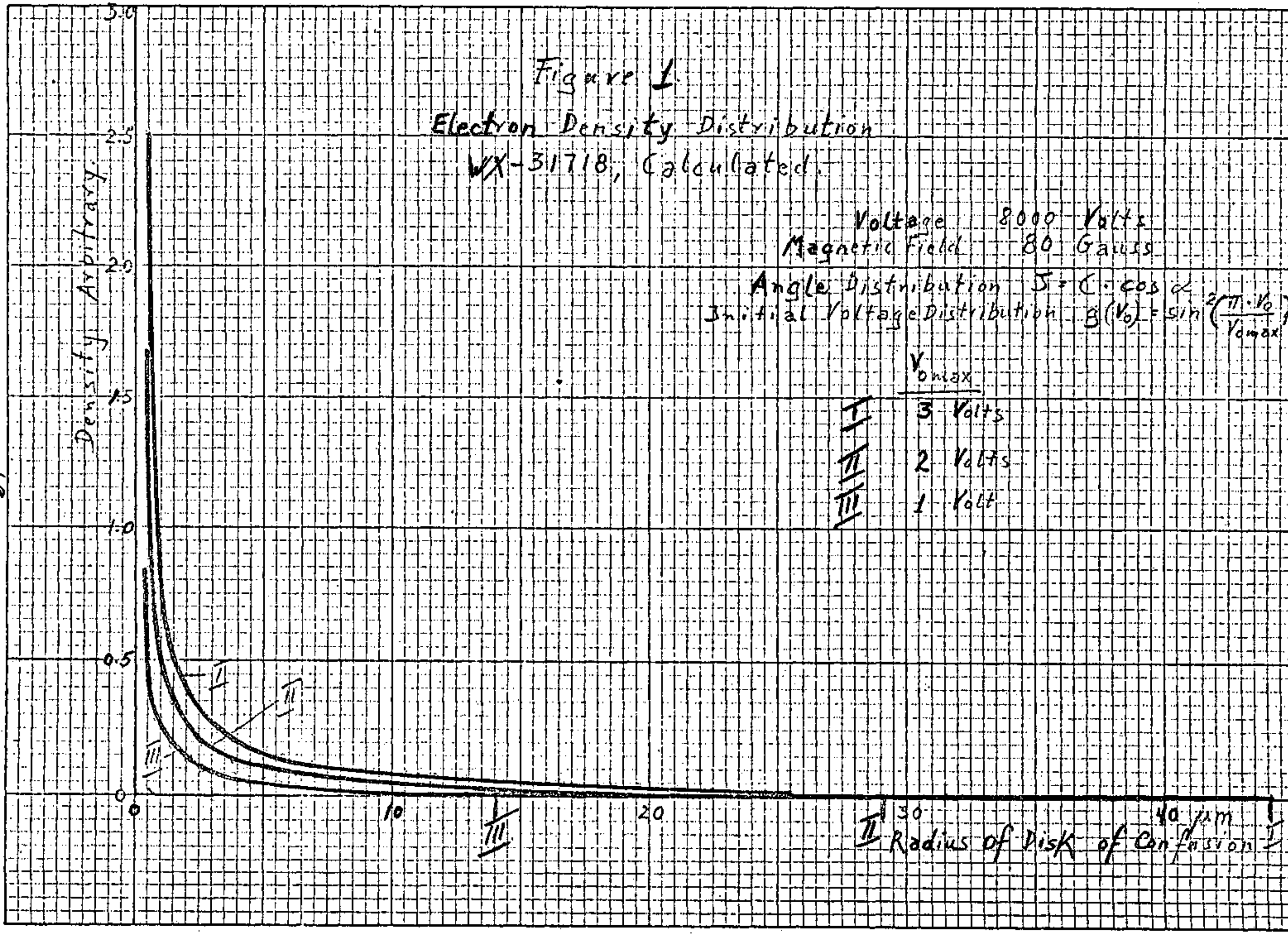
Figure 1
Electron Density Distribution
WX-31718, Calculated.
Voltage 8000 Volts
Magnetic Field 80 Gauss
Angle Distribution J = C · cos α
Initial Voltage Distribution B(V₀) = sin²(π·V₀ / V₀max)
V₀max
I 3 Volts
II 2 Volts
III 1 Volt
Density Arbitrary
0
0.5
1.0
1.5
2.0
2.5
3.0
10
20
30
40
μm
Radius of Disk of Confusion
I
II
III

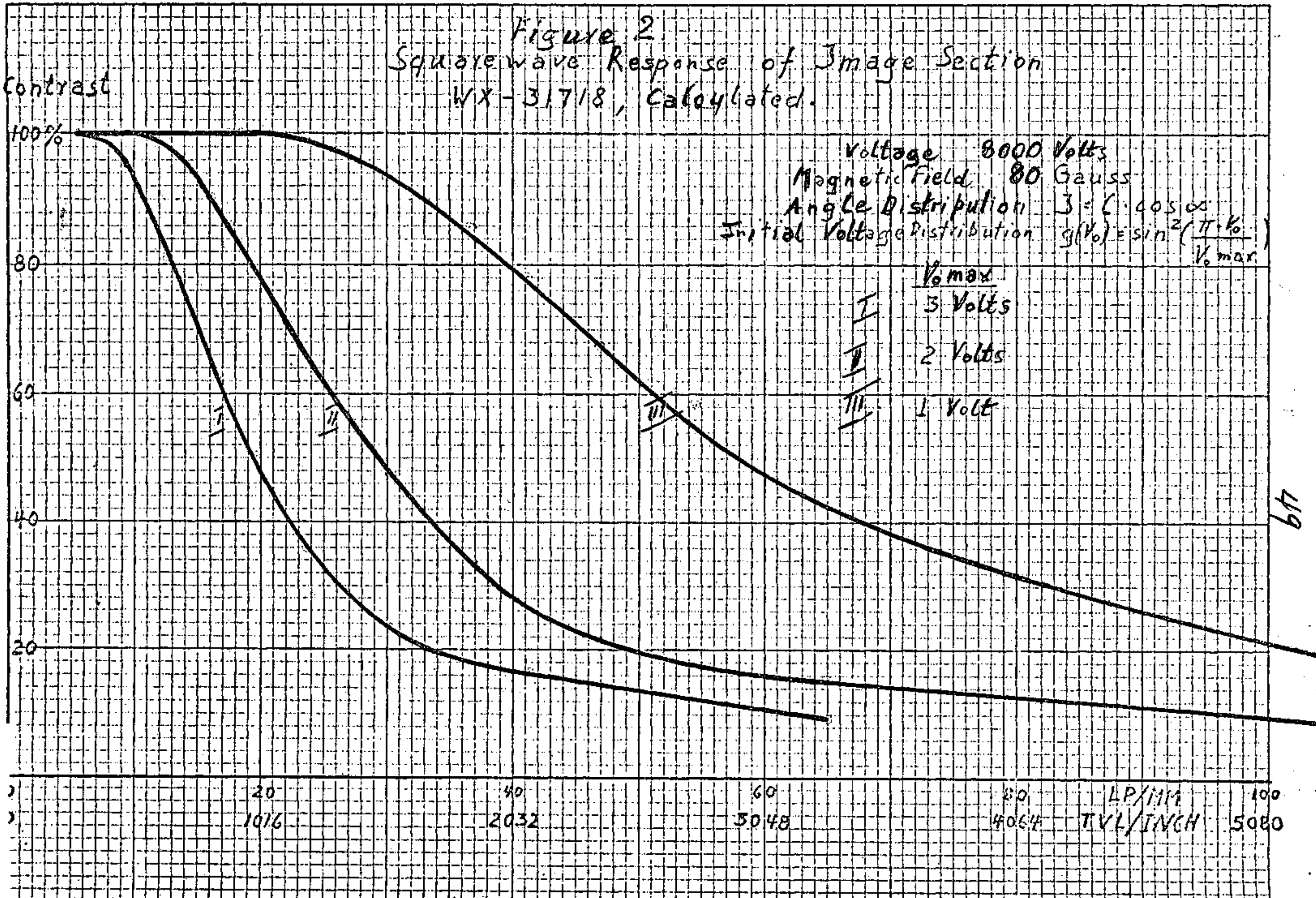

Figure 2
Squarewave Response of Image Section
WX-31718, Calculated.

Figure 2
Squarewave Response of Image Section
WX-31718, Calculated.

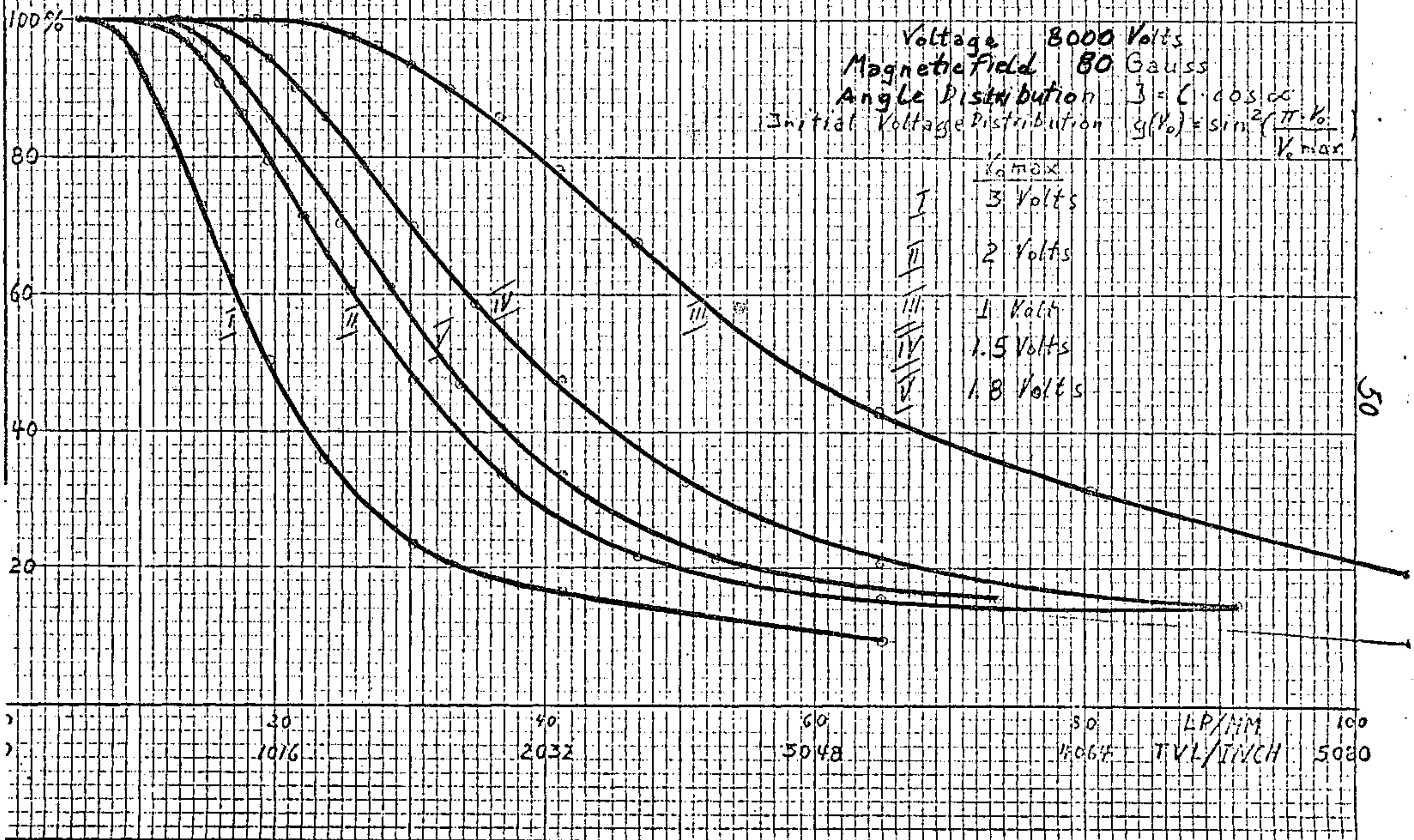

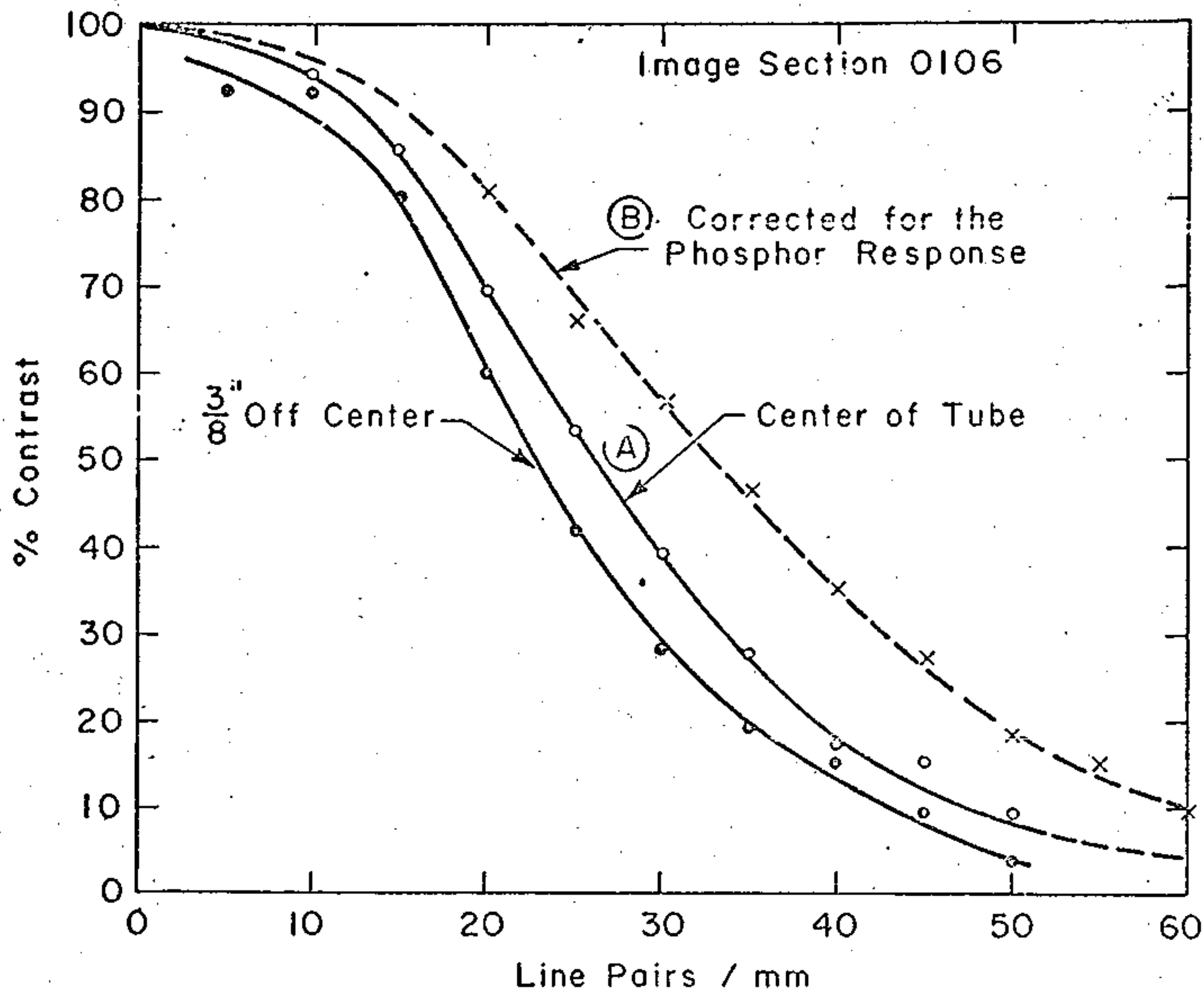

SQUARE WAVE APERTURE RESPONSE
OF AN IMAGE SECTION
FIG. 2.3·17

PHOTOIONIZATION IN GASES
BY G. L. WEISSLER

reprint

INTENTIONALLY OMITTED

APPENDIX III

TARGET RESOLUTION, GUN RESOLUTION AND LOOSE PARTICLES CALCULATION OF COULOMB FORCES

1. Target Resolution

The target resolution is finally limited for extreme thin targets by the size of the KCl particles or fibers and their separation on the substrate. Thicker layers may not be affected as much by the fiber size because the higher number of fibers may smooth out the fiber pattern. A smooth polish surface would give the highest obtainable resolution. However gain and lag would be bad. The fluffier the KCl is, the lower the lag and the higher the gain and needed voltage will be. Thus for high gain and low lag, a fluffy surface is essential. What is done really is that the effective target area is increased many fold. The size of the particles determines the intrinsic resolving power of the KCl layer. Bigger particle sizes will lower the resolving power. If the particles become too big and agglomerate, the target will show graininess because the gain in the center part of the particle is smaller (TSE - Gain). The same thing will occur if one increases the target voltage over a certain limit in which case differences in the gain will show up. A further development of graininess is a crazed target where the foundaries are bright, accepting more beam from the reading gun.

A further limit of the resolution is the so-called blooming effect. This occurs as a spot size increase of the target surface if the spot is changed to the full target voltage. A complete explanation of the definite mechanism for this effect is not available. However, the fact remains that this effect will deteriorate the resolving power of the target independent whether the effect is caused by a long integration or by a high light intensity. A target with a high capacitance will diminish this effect.

In order to improve the resolving power of the KCl target, it would be necessary to make the KCl particles smaller, but still very low density. Now it is a fact that small particles have a tendency to settle denser than big particles. Therefore, an improvement of the resolving power by changing the particle size would always lower the gain and maybe increase the lag. Here the question is how much the intrinsic resolving power would increase with a certain sacrifice in gain. The lag will increase quite rapidly if the layer is made extremely thin, however, a modest increase in lag is not a serious drawback for the intended application. The change in density will have also an effect upon the capacitance. A denser layer of the same amount of KCl will have a higher dielectric constant due to fewer holes, and the layer is thinner. Both may increase the capacitance. However, there is also a difference in the penetration depth of the reading beam. (In the denser material the beam will not penetrate as deeply and therefore will cause a decrease in the capacitance.)

Now considering the blooming effect, one would like to use targets with a high capacitance. The capacitance may be increased by higher density or by less evaporated material, where the latter approach in extreme cases, which may never be reached, would again lower the resolving power.

An entirely new approach to the problem would be the search for a different target material. This might be especially worthwhile because we can relax in the requirement on lag, which originally was one of the major advantages of the KCl layer. (This material must have the same low conductivity, a higher dielectric constant and a higher secondary emission coefficient than the KCl).

Besides this material ought to be easily applied to the target substrate. There are some oxides like BaO, MgO which may be suitable materials for targets. These materials have a higher dielectric constant than KCl and also high secondary emission. However, information on the secondary emission is very sparse and the condition of the tested material is very important so that published coefficients may vary from 4 to 12. I feel that it would be worth while to make some studies in that direction, however, it would take a considerable amount of time to get usable results. Moneywise, it would not be so expensive because most of the work would be done by a technician with the demountable tube and with a simple evaporator. The most promising material would be MgO. It has the highest secondary emission and a very high dielectric constant (of the order of 34 against 5-6 of KCl.). I think that after half a year one would have at least results which would definitely say if this way is feasible. Thus with $15-20K, one can have this information because the equipment is available. These experiments would be carried out with the goal in mind to achieve target characteristics specifically suitable for the Princeton Observatory application.

Summarizing my thoughts on the target improvements, I will say that I see only very little room for improvement of the resolving power of the present target. A small improvement is possible in increasing the storage capacitance by making the material a bit more dense using the same amount of KCl. This would diminish the blooming and enlarge the dynamic range. Lag would go up and the gain slightly down. It might be that the target gain is more uniform and also less susceptible for damages. It is not wrong to try also some variation in the amount of evaporated material. I would not recommend to decrease just the thickness because in this case the particle size may show up more and influence the resolving power and furthermore the target may be more prone to damage. Besides I would recommend to try other materials than gold for the self-stabilization of the target, for instance some semiconductors like germanium and silicon. The most promising approach for improvements would be trials with new materials instead of KCl and here I recommend MgO, also evaporated onto the substrate in a noble gas atmosphere so that it is not dense and then oxidize it. I believe it would, if it is feasible, also be a target less susceptible to damage.

2. Gun Resolution

In the above mentioned report, it was shown that the reading gun contributes very much to the limits of the overall resolving power of tubes with SEC targets. Various causes may influence the performance of the reading gun as there are the electron optical design, the cathode quality and the mechanical design. The electron optical design influences the current density in the spot, the spot size, incident angle of the electrons in the spot, aberrations, beam landing and distortions. The cathode quality influences the current density in the spot and the distribution over the cross section of the spot and the mechanical design will influence distortion, aberrations, current density in the spot and distribution over the cross section.

Let us first consider the cathode. The normal cathode is prone to poisoning by gases and other various influences. The impact of ions during the processing damages often especially the very center part which is the most important emission area for a small spot size. One may get a hollow beam which means a larger spot with less current. An improvement would be the impregnated cathode which is far less susceptible to poisoning, has a better life and is able to deliver higher current densities. For a high performance, it is essential to work in the space charge limited range of the cathode. A poor emitting cathode may work in the temperature-limited range with its center part.

The mechanical design should be mostly directed toward two goals, that all the apertures are aligned perfectly and the center line of the apertures should not be tilted versus the axis or with other words should be normal to the target plane. Both requirements should be improved. The alignment of the apertures can be only improved if the holes are made simultaneously after assembling the triode section of the gun. Here a powerful laser beam may be employed. In order to avoid any tilting, improved assembling fixtures should help.

In the electron optics, I don't think that it would be advisable to make here major efforts, because then one ought to start with an entirely new concept, maybe using a Pierce gun. What I would suggest is, to enlarge the spacing from the cathode to the limiting aperture in order to diminish the angle of incident and apply a .001" aperture. It is important that the beam landing at the target is normal to the target plane. This is not true in the edge region. The poor beam landing at the target edges could be overcome either by a long neck of the gun section, this would diminish the deflection angle, or it can be done electro-optically by a lens in the target region which would work as an after acceleration of the reading beam. However, this would also afford a major design work and would mainly improve the edge resolution and distortion.

Summarizing my recommendations for the gun is the following: The gun should be equipped with an impregnated cathode (Philips cathode). The alignment of the aperture should be improved by punching the holes with a laser beam after assembling. It should be tried to improve any tilting of the gun axis and making the triode section of the gun longer to diminish the gun beam angle at the limiting aperture. Testing the performance and improvement can be done on the demountable tube by means of the monoscope target.

3. Loose Target Particles and Coulomb Forces

During vibration tests it was often observed that particles from the target broke loose. This causes white spots (blemishes) at the target. In the following we will analyze the possible forces which may be involved and indicate if there is a probability to avoid these spots by applying Coulomb forces to the target particles. However, there is the possibility that the breaking loose effect may be instigated by resonance waves across the target. Experiments in that direction will answer finally the mechanism involved.

The Coulomb force on a charged unit area of a plane plate separated by a small distance from an infinite second plane plate so that the separation is small against the extension, what is true for our specific case, is

$$F = \frac{1}{2}\varepsilon\varepsilon_o E^2 \quad \frac{\text{Newton}}{m^2}$$

E = Field strength in $\frac{V}{m}$

ε_o = Dielectric Constant of Vacuum = $8.859.10^{-12} \ \frac{A\ sec.}{V\ m}$

ε = Dielectric Constant, no Dimension

We will now assume a target voltage of 15 Volts and a voltage excursion of the target surface of 5 Volts. The KCl thickness will be 20μm and the dielectric constant approximately 6. So we get for the force

$$F = 3\times 8.86\times 10^{-12}\times \frac{100}{400 \quad 10^{-12}} = \frac{3}{4}\times 8.86 \ \frac{\text{Newton}}{m^2} = 6.65 \ \frac{\text{Nt.}}{m^2}$$

or $F = 6.65\times 10^{-4} \ \frac{\text{Newton}}{cm^2}$

To this force we have to add the adhesive force which is unknown and we well neglect this. If we accelerate the particles say with a rate of 15 g, the force is then 15 times the weight of the material. The weight per unit area is approximately 50 $\mu g/cm^2$, so the force is then

$$F_{accel.} = 15 \times 50 \times 10^{-9} \times 9.81 \frac{\text{Newton}}{\text{cm}^2} = 7.35 \times 10^{-6} \frac{\text{Newton}}{\text{cm}^2}$$

This example shows that the pulling force by the acceleration to 15 g is by a factor of 10^2 smaller than the Coulomb forces. This analysis may suggest to make vibration test with and without charges on the target in order to find out if the pulling forces by the acceleration is the alone responsible mechanism for loose particles.